Chemical and physical properties of the variegated Pluto and Charon surfaces

F. Merlin, M.A. Barucci, C. de Bergh, F.E. Demeo, A. Alvarez-Candal, C. Dumas, D.P. Cruikshank

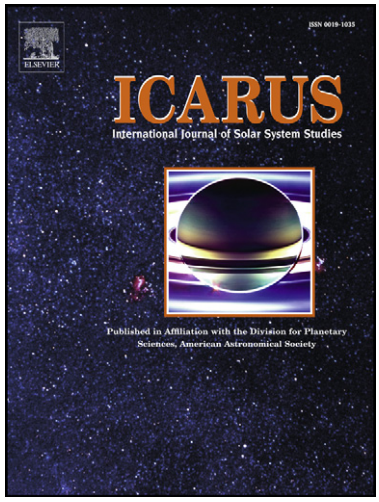

Chemical and physical properties of the variegated Pluto and Charon surfaces

F. Merlin, M.A. Barucci, C. de Bergh, F.E. DeMeo, A. Alvarez-Candal, C. Dumas, D.P. Cruikshank

PII: S0019-1035(10)00308-8
DOI: 10.1016/j.icarus.2010.07.028
Reference: YICAR 9526

To appear in: *Icarus*

Received Date: 27 January 2010
Revised Date: 18 July 2010
Accepted Date: 22 July 2010

Please cite this article as: Merlin, F., Barucci, M.A., de Bergh, C., DeMeo, F.E., Alvarez-Candal, A., Dumas, C., Cruikshank, D.P., Chemical and physical properties of the variegated Pluto and Charon surfaces, *Icarus* (2010), doi: 10.1016/j.icarus.2010.07.028

Chemical and physical properties of the variegated Pluto and Charon surfaces. [1]

F. Merlin,
LESIA/Observatoire de Paris, 5, Place Jules Janssen, 92195, Meudon Cedex, France
Department of Astronomy, University of Maryland, College Park, MD 20742, USA

M.A. Barucci, C. de Bergh, F.E. DeMeo,
LESIA/Observatoire de Paris, 5, Place Jules Janssen, 92195, Meudon Cedex, France

A. Alvarez-Candal, C. Dumas,
ESO/Vitacura, Santiago de Chile, Chile

and D.P. Cruikshank
NASA Ames Research Center, CA, USA

Received _____; accepted _____

Manuscript pages 58; Figures: 17; Tables: 5

ABSTRACT

We present new photometric and spectroscopic observations of the Pluto-Charon system carried out at the VLT-ESO (Chile) with two 8-meter telescopes equipped with the FORS2, ISAAC and SINFONI instruments. The spectra were obtained in the 0.6-2.45μm range with a spectral resolution from 300 to 1500. The SINFONI data were obtained using Adaptive Optics, allowing a complete separation of the two bodies. We derive both objects' magnitudes in the near infrared and convert them into albedo values. These first near infrared photometric data allow to adjust the different parts of Pluto's spectrum, provided by the three instruments. We run spectral models in order to give chemical and physical constraints on the surface of Pluto and Charon. We discuss the dilution properties of the methane ice and its implications on Pluto's surface. The heterogeneities of the pure and diluted methane ice on Pluto's surface is also investigated. The high signal-to-noise level of the data and our analyses may support the presence of ethane ice on the surface of Pluto, which is one of the main products of the methane irradiation and photolysis. The analyses of the spectra of Charon suggest that the water ice is almost completely in its crystalline form and that the ammonia compound is hydrated on the surface of this satellite.

Subject headings: Pluto - Charon - Ice - Spectroscopy

Runningtitle: Pluto and Charon variagated surface.

Corresponding author: Frédéric Merlin

[1]Based on observations made with ESO Telescopes at the Paranal Observatories under programme ID 178.C-0036.

Department of Astronomy, University of Maryland, College Park, MD 20742, USA

E-mail: merlin@astro.umd.edu Phone: +1 301 405 8053

1. Introduction

Among the Trans-Neptunians objects, we find several populations of icy bodies. The system of Pluto, composed of a main body (Pluto) and 3 satellites (Charon, Nix and Hydra), is in resonant motion with Neptune. Pluto is the largest object in the system, with a diameter close to 2150km. Charon, its biggest satellite, has a 1250km diameter while both Nix and Hydra have diameters below 100km. Pluto is largely covered by nitrogen, methane and lesser amounts of CO ice and organic compounds (Cruikshank et al. 1976; Owen et al. 1993). The most recent models (Doute et al. 1999; Olkin et al. 2007; Protopapa et al. 2008) suggest that the methane ice is present in both the pure and diluted states. Charon has an entirely different chemical composition (see Protopapa et al. 2008). Its surface is almost completely covered by water ice, mainly in the crystalline form. An absorption feature close to 2.2 μm was also reported (Brown & Calvin 2000; Dumas et al. 2001; Cook et al. 2007) and is attributed to the presence of an ammonia hydrate.

The presence of large amounts of volatiles species is relatively rare among the different populations of TNOs (see Schaller & Brown 2007, for a detailed model on volatiles escape) and is probably due mainly to the fact that the surface of any atmosphereless object is continuously subjected to space weathering. Strazzulla et al. (2003) and Brunetto et al. (2006), for instance, have shown that irradiated volatile species, containing carbon, are transformed into a refractory crust that is usually dark and featureless. However, the case of the Pluto system is not unique. Eris (Brown et al. 2006; Licandro et al. 2006; Dumas et al. 2007; Merlin et al. 2009), has a surface largely covered by methane ice. This object has two satellites and could be considered the twin system of Pluto. The Haumea system is composed of objects mainly covered by nearly pure water ice (Barucci et al. 2008; Dumas et al. 2009) as well as Quaoar and Orcus, which are the main objects of double systems (Barucci et al. 2008; Jewitt & Luu 2004; Dalle Ore et al. 2009, for instance). All of

these objects exhibit surfaces that are composed of relatively fresh material resulting from different physical processes (sublimation, volatile transport, cryo-volcanism, etc.), and the Pluto-Charon system appears to be the best sample (due to their brightness) to investigate the physical and chemical nature of the biggest TNOs ($\succ$1000 km).

The fresh ice or volatile species give strong constraints on the physical properties of a surface and on the physical processes that govern their evolution. Some of these materials have been analyzed in the laboratory, such as water ice (i.e: Grundy & Schmitt 1998; Mastrapa et al. 2008) or methane ice (i.e: Quirico & Schmitt 1997; Grundy et al. 2002). It is also possible to investigate in detail the temperature or the dilution properties of these different objects and search for surface variation (spatial and/or temporal). The high abundance level of fresh ices or volatile species, as observed on the surface of both objects, provides a great opportunity to search for irradiated products. Some of these irradiated products, at high irradiation levels, are assumed to be similar to the Tholins and black carbons (Khare et al. 1986; Zubko et al. 1996), but other species obtained in the laboratory, such as ethane or ethylene coming from the irradiation of methane ice (Baratta et al. 2002, for instance) are difficult to detect (see DeMeo et al. 2010, or this work).

In this paper, new observations of the Pluto-Charon system are presented. Photometric and spectroscopic data have been carried out at the VLT-ESO with two 8-meter telescopes. Spectroscopic data were obtained from 0.6 to 2.45 μm with a spectral resolution from 300 to 1500. The high spectral resolution and the high signal-to-noise ratio, the best published until present, allow us to investigate the physical and chemical properties of both objects. In the first section, we present the observations and the data reduction procedures. In the second section, we present the results on the absorption features and some results on the chemical composition of the surface of Pluto and Charon. We discuss the dilution properties of the methane ice and compare our results with previous ones. We also search

for irradiated products, such as ethane and ethylene compounds, which are produced by the irradiation and photolysis of methane ice. These observations are a part of the Large Program 178.C-0867(L)

2. Observations and data reduction

The observations of Pluto and Charon have been performed with the VLT (Very Large Telescope) at ESO (Chile). Near-infrared (IR) photometry and spectroscopy were carried out on 2008 April 12 and April 13 with ISAAC (http://www.eso.org/instruments/isaac) installed on UT2 and SINFONI (http://www.eso.org/instruments/sinfoni) installed on UT4. We also carried out visible spectroscopy on 2008 April 12 with FORS2 (http://www.eso.org/instruments/fors2) installed on UT2. Table 1 lists the details of the observational circumstances. Because the Pluto-Charon system is a tightly-coupled body from ground-based observations, and was partly unresolved in the visible and in the J band, we explain our procedures to derive accurate photometry of both objects in the near-IR and our attempts to derive a complete spectrum of each object from 0.6 to 2.45 μm.

Table 1 must appear here

2.1. FORS2

The data in the visible range were obtained on 2008 April 12 with FORS2, the grism 300I and a 1" slit that allows us a spectral resolution close to 300 in the 0.6-1.00 micron range. The data reduction in the visible range has been performed with the GASGANO software, version 2.2.7, that takes into account the bias and flat-field correction. The wavelength calibration was performed using the OH and Fraunhofer spectral lines. The angular separation between the two objects was close to 0.8" and the position of the

two objects compared to the parrallactic angle was optimal to detach the spectrum of each other. The observational circumstances should allow us to disentangle both spectra (seeing was near to 0.4" and the airmass close to 1.0). The spatial separation of Pluto and Charon is presented in Figure 1. A part of the flux of each object contaminates that of the companion. We try to remove the part of each other using the assumption that the distribution of the flux of each object along the spatial direction has a Gaussian profile.

Figure 1 must appear here

The flux of Charon is extracted as 2 times the flux from pixels 118-123 along the spatial axis minus 2 times the flux from pixels 107-112 along the spatial axis (containing the background signal and that of Pluto). The flux of Pluto is extracted from pixels 108-122 along the spatial axis. We subtract the flux of Charon, previously computed and subtract the background signal from two windows that are located on both sides of the objects flux, far enough to avoid flux contamination. The results of the spectra extraction are presented in Figure 2. Our method appears limited in the case of Charon. Indeed a blue slope is added in the spectrum of Charon, due to an obvious flux contamination of Pluto. Assuming there is also reverse contamination, the slope of Pluto is corrected with the colors provided by Buratti et al. (2003) with V-R=0.57 and using a linear regression on our spectrum from the 0.6-0.7 μm range to extrapolate the flux at 0.55μm.

Figure 2 must appear here

2.2. SINFONI

In the H and K bands (1.45 to 2.45 μm), we use the SINFONI instrument and the H+K grism to perform spectroscopy of both objects with a spectral resolution of 1500, a plate scale

of 100 mas per pixel and the adaptive Optics mode. The FWHM on the frames dropped below 0.15" during both nights and it was possible to separate both objects (see Figure 3). The data reduction was performed with the software GASGANO, version 2.2.7, and the spectra were extracted from the individual data using QfitsView, the three-dimensional visualization tool developed at the Max Planck Institut fur Extraterrestrial Physik for SINFONI (http://www.mpe.mpg.de/ott/QFitsView). The wavelength calibration was performed using Xenon, argon, krypton lamps and telluric spectral lines. For both nights, we verified that the contribution of Pluto's flux into that of Charon is smaller than 3%.

Figure 3 must appear here

Two different spectral analogs were used for calibration. HD147935 is a G5V spectral type and SA 110361 is a G2V. The division of the spectrum of SA110361 by that of HD147935 shows small variations. Except for a slightly redder slope for the second star in the H band (3%/100nm in the beginning of the H band), the differences are less than 2% over the entire wavelength range. These differences are compatible with those found with the model of Pickles (1998) when the spectrum of a standard G2V star is divided by that of a standard G5V star. This means that the differences implied by the airmass variations are probably very small, and apparently smaller than the differences coming from the different spectral types of the analog stars. In all cases, we identified the possible differences in the data reduction and verified that they remain small. The spectra of Charon and Pluto are presented in Figure 4 and Figure 5 and some characteristics of the spectroscopic observations are summarized in Table 2.

Table 2 must appear here

Figure 4 must appear here

Figure 5 must appear here

2.3. ISAAC

Near-IR observations were carried out under good photometric conditions with ISAAC. Photometric J, H and Ks measurements (centered at 1.25, 1.65 and 2.16 μm, respectively) were carried out on 2008 April 13. The calibration was performed by observing several faint standard stars during the ESO calibration procedures that bracketed the airmass of Pluto-Charon. The data reduction was performed using the MIDAS package and the data processing method follows that described in Romon et al. (2001).

In the J band, the spectroscopic observations were done during the second night and the angular separation drops to nearly 0.4". Because the position of Charon compared to that of Pluto was not along the parrallactic angle, we were not able to separate the spectra from each other. We use the SW mode of the instrument with a 1" slit, giving a spectral resolution of about 500. The observations were done by nodding the object along the slit by 10' between two positions, named A and B. Each pair of A and B images was combined using the MIDAS package following the procedures described by Barucci et al. (2002). The wavelength calibration was performed using xenon and argon lamps and telluric spectral lines. The spectrum obtained in the J band (from 1.1 to 1.35μm) is presented in Figure 6.

2.4. Magnitudes extraction

As it was not possible to separate the flux of each object with ISAAC, we use our results obtained with the SINFONI instrument to compute the relative flux of both objects in the H and K bands. The separation between Pluto and Charon was better the first night and we use this night as reference. The ratio $\frac{Light_{Pluto}}{Light_{Charon}}$ is conserved during the first night

for different extraction windows, from a 3 to 7-pixel radius. Similar extraction windows (3-5pixels) have been used during the second night to measure the ratio $\frac{Light_{Pluto}}{Light_{Charon}}$ at the time of the ISAAC photometric observations.

The total flux of the spectra, before division by that of the analogue star, is convolved with the response curve of the ISAAC instrument in both H and Ks filters. The response curves are available online (http://www.eso.org/sci/facilities/paranal/instruments/isaac/inst/isaac-img.html) and take into account the wavelength ranges outside the telluric regions. After this operation, we compute the ratio of the flux of the two objects in both bands. We obtain the following contribution for Pluto and Charon in the H and Ks bands, respectively: 0.873/0.127±0.003 and 0.856/0.144±0.005. The differences between both objects, in terms of magnitude, are 2.09±0.04 in the H band and 1.94±0.05 in the Ks band. The magnitude for the entire couple is known for the second night with ISAAC and we derive the following magnitudes: H_{Pluto}=13.05±0.05, H_{Charon}=15.14±0.05 and Ks_{Pluto}=13.29±0.06, Ks_{Charon}=15.21±0.06. In order to separate the magnitudes in the J band, we use a spectral model (see section on the spectral modeling) obtained from the H+K part only, assuming that the chemical composition is consistent in the J, H and K parts. Indeed, the spectral behavior of ices and of organics and carbons that have a linear continnum, are quite dependent in these wavelength ranges. However this approach is not perfect as well as the fit of the methane ice bands present on the spectrum of Pluto which may add some uncertainties at second order. Using the spectral models for both objects, we compute the ratio, in terms of reflectance between the J and H bands. We find the magnitude ratios J/H = 1.20 for Pluto and 1.28 for Charon. (i.e.: J_{Pluto}=13.14 and J_{Charon}=15.16). The summation of both magnitudes is 12.99, which is close to that measured for the entire couple with ISAAC; 12.97±0.04. This gives us a good confidence level of our method and results, summarized in Table 3.

In order to adjust the visible spectrum with the J and H+K spectra, the visual magnitude of both objects is needed. FORS2 data of the Pluto/Charon system do not allow to resolve the two objects, and it is not possible to adopt the approach used for the H and K bands. The use of spectral models is not possible either because of a lack of correlation of the spectral behavior of the organics between the visible and the near IR. We use values previously published in the literature in order to solve this issue. Buie et al. (1997) used observations with the Hubble Space Telescope to provide accurate light curves of Pluto and Charon. From this work, we derive the mean magnitude in the V band: m_V=15.47 and 15.37 for Pluto and we find the mean m_V =17.27 and 17.31 for Charon, for the first and second night, respectively. Using the mean V magnitude for r=39.5 AU and Δ = 38.5 AU at zero phase angle, we derive the following magnitudes: m_V=14.56±0.03 and 14.46±0.02 for Pluto and m_V=16.46±0.04 and 16.50±0.04 for Charon compared to our observational circumstances (r=31.44 AU, Δ = 31.06 AU, α=1.65°). These results imply that the magnitude differences between V and J equal 1.80 and 1.96, respectively for the two nights. Our results coming from the H and Ks parts give different results, with smaller variations. This could be due to a different light curve amplitude in the near IR, or/and a light curve variation between 2008 and 1993. Buratti et al. (2003) showed that the light curve amplitude of the Pluto-Charon system should drop between 1993 and 2008 (from 0.31±0.01 to 0.26±0.02) given the heterogeneous nature of Pluto's surface and the viewing geometry (the pole angle inclination is passed from -10 to -41° between 1993 and 2008). Since the contribution of the bright south polar cap is more important, whatever the viewing longitude, Buratti et al. (2003) expect that the light curve amplitude should decrease and that the albedo of Pluto should be greater in the next 30 years. Our near IR observations support the hypothesis on the light curve amplitude decrease but similar observations in the visible must be performed to firmly confirm these results. We convert the photometric values into reflectivity, as described in Merlin et al. (2009). In Figure 6, the

different spectra of Pluto (obtained in the visible during the first night and in the near-IR the second night) are then converted in reflectance and normalized with the results obtained in the R, J, H and Ks photometric bands. **The wavelength range of our J spectrum is shorter than the bandwidth of the photometric J filter. The spectral model used to compute the J/H magnitude ratio allows us to take into account the lack of spectral data in the borders of the filter bandwidth in order to convert the J spectrum into reflectivity.**

Table 3 must appear here

Figure 6 must appear here

2.5. Albedo extraction

In order to reduce the errors in terms of albedo, we directly compute the albedo of the object in the near IR. The following relation from Jewitt & Luu (2001) is used for this purpose:

$$\Phi(\alpha)\times \mathrm{Alb}\times \mathrm{D}^2 = 8.96\mathrm{E}^{22}\times \mathrm{R}^2\times \mathrm{Dis}^2\times 10^{(0.4(msun-mObj))}$$

where the phase function $\Phi(\alpha)$=1.05 and 1.14 for Pluto and Charon, respectively (Buie et al. 1997), the diameter is $\mathrm{D}^2=5.5225\mathrm{e}^{12}$ meters for Pluto and $1.459264\mathrm{e}^{12}$ meters for Charon, the heliocentric distance is $\mathrm{R}^2\mathrm{Dis}^2=31.44^2\times 31.06^2$ UA, the solar magnitude in the H band is mSun=-28.01, that of Pluto is m_{Pluto}=13.05 and that of Charon is m_{Charon}=15.14. The calculation gives: Alb_{Pluto}=0.56 and Alb_{Charon}=0.28 in the H band. We derive the V albedo for Pluto with the previous assumption for the V magnitude: Alb_V=0.53, that is consistent with the work of Buie et al. (1997).

3. Spectral analyses

3.1. Charon

On the spectra of Charon (see Figure 4), the deep absorption features centered at 1.5, 1.65 and 2.0μm are attributed to the presence of crystalline water ice (Brown & Calvin 2000, for instance). We confirm the presence of the weaker absorption features at 2.0 and 2.2μm, discovered by Brown & Calvin (2000) and assumed to be likely relative to the presence of ammonia (Dumas et al. 2001; Cook et al. 2007). The band at 2.0 μm is not fully reliable due to close telluric CO_2 bands (1.961, 2.009 and 2.060 μm, see Goldberg et al. 1948). Our data are taken one day apart (difference close to 60° in longitude). As the sub-solar point is far from the equator of the planet (Pluto's pole is inclined by -41°), only 26% of the surfaces of both objects have changed between the two nights. During the second night, we observed the Anti-Pluto surface of Charon. Except in the telluric bands, minor modifications in the shape and in the depth of the absorption bands can be detected in both spectra (below 5%, see Figure 4). At 2.21μm, we report the following absorption band depths: 8.14±2.99% for the first night and 5.36±1.02% for the second one. The band depths and positions were fit with a Gaussian curve and the errors correspond to 1sigma of the spectral noise in the same wavelength range (see Figure 7 for instance). It seems that the continuum of the 2.2-2.3-micron region is higher and the absorption band at 2.21μm is slightly deeper for the first night but it is not very significant within the errors. The feature located close to 2.21 μm has been attributed to ammonia or hydrated ammonia (e.g.: Cook et al. 2007; Moore et al. 2007). Moore et al. (2007) and Cruikshank et al. (2005), summarize the different possible absorption bands, for the ammonia ice, ammonium hydroxide, and ammonia hydrate. On the spectra, the absorption band is located at 2.2111±0.0009μm (FWHM: 0.0298±0.0109μm) and 2.2122±0.0010μm (FWHM: 0.0261±0.0050μm). These measurements are slightly different from those reported by Cook

et al. (2007) for the anti-Pluto surface (2.2131±0.0007 μm, FWHM:0.0188±0.002μm), which suggests a probable variation of the chemical composition. Our observations favor the presence of the monohydrate NH_3:H_2O among the hydrates, a mixture of NH_3+H_2O or the ammonia hydroxide NH_4OH. The ammonia hydroxide and diluted NH_3 have a moderate absorption feature at 1.65μm (i.e: Cruikshank et al. 2005). However, the 1.65μm feature of our spectra is very deep, as deep as the main feature at 1.4-1.6μm, which is the case in spectra of pure crystalline water ice at temperature appropriate for Charon. Therefore only small amounts of ammonia are then expected, but optical constants of monohydrate NH_3:H_2O in this wavelength range are required to confirm this hypothesis. The presence of NH_4^+ is suggested by Cook et al. (2009) from the detection of an absorption feature near 2.24 μm. NH_4^+ could be produced from irradiated H_2O/NH_3 mixtures. This feature is not detected in our observations and we expect that this compound is less abundant on the Anti-Pluto surface.

Figure 7 must appear here

3.2. Pluto

The spectrum of Pluto is mainly composed of the methane absorption bands, which appear from 0.72 to 2.42μm (see Figure 2 and Figure 5). There is the unambiguous 1.689-micron band reported by Quirico & Schmitt (1997), attributed to the presence of pure methane ice. The absorption band of N_2 at 2.15μm is rather weak but well defined. The main absorption feature of CO ice (Quirico & Schmitt 1997) is also present at 2.352μm as well as the weaker ones at 2.405μm and 1.578μm. However, the 2.405μm feature is not expected to be entirely CO (see DeMeo et al. 2010) and the 1.578μm feature seems too deep compared to the 2.352μm band that has a much bigger absorption coefficient (see Section 4.5). The 2.318, 2.337 and 2.409μm bands of ^{13}CO are too weak to be detected. Similarly

to Charon, the differences between the two nights are very small (usually within 5% and close to 10-15% in the deepest absorption bands in the K band).

Determining the position of the methane ice bands is helpful to constrain the dilution state of the methane ice. The method to measure the position peak is described in Tegler et al. (2008). The shifts of the methane ice bands compared to those of pure methane ice seem to be in agreement with a diluted methane ice in a nitrogen matrix (see Figure 8 and Table 4). Our results give slightly different peak positions compared to the results of Licandro et al. (2006) on two absorption bands measured in the visible (0.7290μm and 0.8885μm instead of 0.7284$\pm$0.0004μm and 0.8877$\pm$0.0005μm in this work). In Doute et al. (1999), the authors report variation of the peak positions in the near IR. These observations confirm the heterogeneity of the surface of Pluto. The wavelength shift is dependent on the wavelength, as observed for diluted methane ice (with CH_4:$N_2 \leq 0.02$ for instance, see Figure 8). The mean dilution level is obviously weaker but the dilution state seems to be constant along the path of the light into the surface. Stratification of pure and diluted methane seems to be less important compared to the case of Eris (Merlin et al. 2009) where the wavelength shift primarily depends on the absorption band depth in the visible, showing an obvious stratification of the diluted methane ice on the sub-millimeter surface of this object. We clearly observe pure methane ice on the surface of Pluto, this suggests that the pure and diluted methane ice are also spatially (horizontally) separated on the surface and not only vertically stratified. This result confirms the presence of pure methane ice patches on the surface of Pluto, expected by Doute et al. (1999) and Lellouch et al. (2009). Volatile transport may take place if we take into account previous results that show stratification of the methane (Doute et al. 1999). A complete coverage of the surface of Pluto is required to deal with the heterogeneous nature of this dwarf planet. No spectral variations are observed on the two different spectra. The differences of the peak positions between the two nights are very small (below 0.0005μm) and they are not constant.

Figure 8 must appear here

Table 4 must appear here

4. Spectral models

4.1. Modeling description

In order to investigate the chemical properties of the surface of these objects, we use the spectral model developed by Hapke (1981, 1993). This model allows us to determine the reflectance spectra or the albedo of a medium from individual physical properties of the different chemical components. The albedo is approximated using the Equation 44 of Hapke (1981):

$$Alb = r_0(0.5 + r0/6) + (w/8)((1 + B_0)P(0) - 1)$$

where w is the single-scattering albedo and r_0 the bihemispherical reflectance, which is purely single-scattering albedo dependent:

$$r_0 = (1 - \sqrt{1 - w})/(1 + \sqrt{1 - w})$$

w depends on the optical constants and the size of the particles and is computed for a multi-component surface (assumed to be intimately and/or geographic mixed, see Poulet et al. 2002). B_0 is the ratio of the near-surface contribution to the total particle scattering at zero phase angle and P is the phase function. The method follows the instruction delivered in Merlin et al. (2009), that assumes an albedo approximation model with a phase angle equal to 0 and B_0 is assumed to be close to 0.67 for icy objects (Verbiscer & Helfenstein 1998). The surface roughness and interferences are negligible. The phase function is approximated by a single Henyey-Greenstein function with different asymmetry parameters ξ as:

$P(0,\xi) = (1-\xi^2)/(1+2\xi+\xi^2)^{3/2}$

The free parameters are the particle size and the ratio of the different compounds in the mixture. We use a best fit model based on the Levenberg-Marquardt algorithm in order to minimize the reduced χ^2. The minimization is applied outside the telluric absorption bands which can affect the results. As the differences between the two nights are weak, we decide to model only the spectra of Charon and Pluto taken during the second night, where the signal-to-noise level is superior.

4.2. Pluto's modeling

We consider the following types of chemical compounds for Pluto: pure methane ice (40K, from Quirico & Schmitt 1997), diluted methane and CO in nitrogen ice (with 0.36% of CH_4 and 0.10% of CO at 36.4K, see Quirico & Schmitt 1997), diluted methane ice in nitrogen (without diluted CO), Titan Tholin (Khare et al. 1986) and amorphous carbon (Zubko et al. 1996). Other irradiated products, as ethylene or ethane (see Merlin et al. 2009, for a discussion on the irradiated products) could be present on the surface of Pluto, so we add these compounds in our models, unfortunately obtained at 21K, from Quirico & Schmitt (1997). This temperature is lower than expected on the surface of Pluto (∼50K). DeMeo et al. (2010) report that C_2H_6 on Pluto is probably not in its amorphous state. At low temperature, the ethane ice is in amorphous state (21K) and is transformed into its metastable or crystalline state at higher temperatures (between 30 and 55K and greater than 60K, respectively according to Hudson et al. 2009). Small wavelength shifts and surface area changes could occur, depending on the phase. For instance the absorption band centered at 2.402μm in amorphous phase conditions moves to 2.404 and 2.406μm for metastable and crystalline forms, respectively (see Hudson et al. 2009).

Figure 9 must appear here

Previous authors used different methods to model the Pluto's surface (intimate, intra-mixtures, stratification, geographic) with similar success. Since patches of pure and diluted methane ice have been suggested, we consider in this work an areal mixture model. In this model, presented in Figure 9, the surface is a combination of two areas. The first area (15% of the surface) is composed of 79% of pure methane ice (57% and 12% with particle size of 2mm and 6cm, respectively), 19% of Titan Tholin (2.5μm) and 2% of amorphous carbon (10μm). The second area (85% of the surface) is composed of 79% of diluted methane and carbon oxide in nitrogen (with particle size of 20cm), 19% of Titan Tholin (2.5μm) and 2% of amorphous carbon (10μm). In both areas, the chemical compounds are intimately mixed. As discussed by Grundy & Buie (2001), the big grains simulated in our models should be more relative to aggregates of sub-millimeter size particles.

The use of small and large particle sizes serve to fit the deep and broad bands, which it is not possible with only one particle size. According to Grundy & Buie (2001), the small grains could represent rough texture on the surfaces of the large ice grains. This model agrees to the data mainly within 5-10%, except few cases and close to the telluric absorption bands. A better accuracy on the albedo in the visible part is required to adjust this part with that of the near IR, in order to improve the agreement between the synthetic and object spectra. Refinements of the models are also required to improve the agreement close to the pure methane ice band (1.689μm) and that of the CO band (2.35μm), for instance. The CO band at 2.35μm is overestimated in our models, suggesting smaller amounts of diluted CO on the surface of Pluto. Red and dark materials, such as Titan Tholin, need to be intimately mixed with bright compounds (N_2 or CH_4) to match at the same time, the red slope in the visible, the strong absorption features in the K band (with nearly saturated CH_4 bands) and the high albedo level of the spectrum in the continuum.

The model needs to be refined to better fit the different absorption bands of methane ice. These discrepancies could be partly due to the larger uncertainties on the optical constants, obtained from laboratory measurements on millimeter-thick samples, in these wavelength ranges. Models including stratification of methane ice with different particle sizes could be helpful in this purpose. Unfortunately, this type of model has been performed by Doute et al. (1999) with similar problem. At the first order, our results are fairly close to those performed by previous authors (Olkin et al. 2007; Protopapa et al. 2008; Grundy & Buie 2001, for instance). Indeed, pure and diluted methane ice in N_2 are needed, as well as small amount of dark compounds. Different particle sizes, with relatively small and large sizes, are required to fit the weak and strong absorption bands of methane. The particle size of diluted methane ice is larger than that of pure methane ice, confirming all the previous results. In detail, the ratio pure:diluted methane ice is different but this could be generated by differences in the initial conditions. The asymmetry parameter equals -0.43 in this work, instead of -0.3 in the work of Protopapa et al. (2008) and Olkin et al. (2007) for instance, and we neglect the surface roughness. Differences are also caused by the use of a different albedo, measured and computed in the H band, and the addition of the 0.6-1.0μm band. However, this work agrees with the previous results. Adding these new data allows us to better constrain the size of Titan Tholin, for instance. The particle size of this compound is expected to be smaller than suggested by previous authors (close to $\sim$2μm instead $\sim$10μm).

4.3. Charon's modeling

For Charon, we use crystalline and amorphous water ice (at 50 and 38K, respectively), a blue component and different ammonia species. Unfortunately, optical constants of monohydrate NH_3:H_2O are not yet available on our complete wavelength range. We use optical constants of hydrated ammonia, with 3% of ammonia diluted in water and cooling

at 77K (Brown et al. 1988). The continuum of Charon (observed at 1.45, 1.8 and 2.25μm) has a negative slope (i.e. blue slope). It could be due to the presence of abundant amounts of amorphous water ice (see Merlin et al. 2007) or the presence of a blue component. As the 1.65μm absorption band is strong, the abundance of amorphous water ice should be low compared to the crystalline one and the blue slope is probably due to an unidentified component. To confirm this hypothesis, we develop a method to determine the ratio $H_2O_{amorphous}/H_2O_{crystalline}$. The method consists of computing the ratio, in terms of absorption band depth and surface area, between the entire 1.5-micron and 1.65-micron bands. These measurements are compared to those obtained with different mixtures of crystalline and amorphous water ice for different ratios and particle sizes (see Figure 10 for an example with 50% of each state with similar particle sizes of 10 or 100μm). The ratio is used to eliminate the possible presence of dark and featureless compounds that can modify the depth of the two bands. We divided the spectrum by the continuum, adjusted by a linear regression between 1.45 and 1.70μm for the large 1.5μm band and between 1.62 and 1.69μm for the 1.65μm band. The different mixtures of water ice are created with the spectral model presented in this paper. We use both intimate and geographic mixtures and optical constant data of amorphous and crystalline water ice from Grundy & Schmitt (1998) and Mastrapa et al. (2008) for different temperatures (from 30 to 70K), in order to cover a wide range of possibilities. Our method is based on the assumption that amorphous and crystalline particles have similar sizes. However, different particle sizes (up to a factor of 10) give relatively similar results for geographical mixtures. In the case of intimate mixtures, the value given by our method is a lower limit of the crystalline water ice fraction if the amorphous particles are greater than the crystalline ones. To conclude, except for the case of intimate mixtures with crystalline particles much larger than the amorphous ones, the method can give, with good accuracy, the lower crystalline fraction in the H_2O_{cr}:H_2O_{am} mixtures. Particle shapes may also affect band characteristics but these effects are not yet

constrained neither from laboratory measurements nor spectral modelling.

Figure 10 must appear here

Our measurements give a ratio of the absorption band depth (1.5μm/1.65μm) of 1.4±0.08 and a surface area ratio of 6.8±0.8. Compared to the different synthetic spectra, this implies a lower limit of 90% of crystalline water ice (see Figure 11 on the surface area ratio for example) if the particle sizes are smaller than 100μm and the temperature close to 50K. If crystalline particles are 10 times larger than the amorphous ones, we expect a minimum of 80%. Hydrated ammonia could induce small spectral changes in the 1.45-1.70μm range (see Figure 10). The main effect is to reduce the depth and the surface area of the 1.65μm band (Brown et al. 1988) which could lead to an underestimation of the crystalline water ice abundance. Therefore, the water ice is supposed to be entirely, or at least mainly, in its crystalline form. This confirms our previous assumption and means that the blue slope is probably due to the presence of an unknown blue compound.

Figure 11 must appear here

We assume optical constants of a blue component with no absorption bands in the 1.5-2.5μm range that has a similar spectral slope compared to that of the kaolinite, a hydrated silicate (phyllosilicate). Optical constants are crudely approximated using the theory of Hapke (1981) with a constant real index of refraction (n=1.4). From iterations and for each wavelength, we compute the best imaginary part of the refraction indices (k) considering the following equation:

$$ref_{compound} = S_e + (1 - S_e)\frac{(1-S_i)\Theta}{(1-S_i\Theta)}$$

where S_e, S_i and Θ are the surface scattering (external and internal, respectively) and absorption coefficients. All of these coefficients depend on n and/or k. They are

defined in Hapke (1981). The reflectance of the kaolinite comes from the ASTER database (http://speclib.jpl.nasa.gov/search-1/mineral) and we use a polynomial curve to deduce the reflectance of that compound with no absorption features. The imaginary part of the refraction indices (k) as well as the reflectance are presented in figure 12. Spectral features of aqueous altered minerals have been identified on different TNOs (see de Bergh et al. 2004, for instance). We assume that similar compounds, such as phyllosilicates, can be present on the surface of Charon. However, the constructed blue component could be also considered as an ad hoc compound.

Figure 12 must appear here

The spectral model suggests the presence of 43% of crystalline water ice (33 and 10% with particle size of 60 and 200μm, respectively), 27% of hydrated ammonia (31μm), 18% of amorphous carbon (10μm) and 12% of the blue component created previously (with a particle size assumed to be close to 12μm) on the surface of Charon. All compounds are intimately mixed. The errors between the synthetic and object spectra are within 5% except close to the telluric absorption bands (see Figure 13). The results of the models are in agreement with our previous analyses and support the presence of large amounts of crystalline water ice and a small amount of hydrated ammonia (less than 3% of ammonia is present in the hydrated ammonia, and the total percentage of ammonia on the topmost layer of Charon is close to 1%). Even if the main absorption bands are fitted well, a wavelength dependent phase function, not used in this work, seems to be required. The ratio H_2O/carbon is not definitive because it is dependent on the unknown initial conditions (asymmetry parameter equals -0.2, for instance). Refinements to the model could increase the agreement between the model and the data, and give more physical constraints on the surface of Charon.

Figure 13 must appear here

4.4. Search for irradiated products

DeMeo et al. (2010) search for the presence of ethane on Pluto's surface by modeling a spectrum of Pluto in the near IR wavelength range. They detect several features in the data at the locations that ethane absorbs that are not accounted for by methane, nitrogen, or CO, suggesting the presence of a small amount (no more than a few percent) of pure ethane. In order to confirm and constrain the amount of irradiated products, such as ethane and ethylene, we ran different spectral models including these compounds. The strongest absorption features of ethane and ethylene are observed in the 1.5-2.4μm range in our data (see Merlin et al. 2009, for a detailed discussion). We process the different models in the H and K bands, independently, to increase the accuracy of the models and effects of both irradiated compounds on the results. Indeed, if we use broad wavelength range, the models are quite insensible to these compounds which exhibit weak and narrow absorption bands. The results of the spectral models with ethane ice are presented in figures 14 and 15 (upper parts). In both cases, there is good agreement between the models (obtained with intimate mixtures) and Pluto's spectrum (within a few percent). However, in the H band, only 3% of ethane (100μm) is used and the results are very similar to those obtained without this compound (see Figure 14). The reduced χ^2 is 17% greater without ethane. In the K band, 5% of ethane (700μm) is used and the fit is significantly better, see Figure 15 (reduced χ^2 7 times greater without ethane) but the fit is less accurate than in the H band and the models need improvement. These results suggest that a small amount of ethane may exist on the surface of Pluto but no more than 5% on the observed side. In both cases, the particle size of ethane is smaller than a few hundred μm, significantly smaller than that of methane grains. Using the same approach, we do not detect any evidence of the presence of ethylene. Observations, suggesting that ethane seems more abundant than ethylene,

have also been performed on Eris by Merlin et al. (2009). These authors propose that the proton irradiation and UV photolysis are perhaps the most preponderant on Eris among the different irradiation processes according to laboratory experiments performed by Baratta et al. (2002). Similar conclusions can be drawn for Pluto.

Figure 14 must appear here

Figure 15 must appear here

The detection of the ethane absorption bands is more obvious when we measure the differences between the synthetic spectra without C_2H_6 with that of Pluto in the K band. Indeed, these results reveal the absorption bands of C_2H_6 (see Figure 15, lower part). The synthetic spectra have been composed of pure methane ice (shifted to match the diluted methane ice bands) or of diluted CO and CH_4 with and without ethane. The agreement is good between the data and these models, except for the range close to 2.35 μm for the model with no CO, and close to 2.40μm where the models are lower than the object spectrum. These results confirm the previous detection of ethane at 2.274, 2.297, 2.315 and 2.403μm by DeMeo et al. (2010) and confirm that the 2.35μm band is mainly due to the presence of CO. The signal-to-noise level of our data is better than that of DeMeo et al. (2010) and it is possible to report the absorption bands depth and position of some C_2H_6 spectral features (see Table 5). It is possible to identify the state of the ethane ice from different bands located near 2.274 and 2.404μm for instance (Quirico & Schmitt 1997; Hudson et al. 2009). The measurements suggest that ethane ice is probably in its metastable or amorphous phase. However, the measurements performed on the ethane sample by Quirico & Schmitt (1997) at 21K, corresponding to the amorphous phase, match those of Hudson et al. (2009) performed on ethane samples in its metastable phase. In order to constrain the state of ethane, new laboratory measurements as well as better signal-to-noise observational data are needed. If the peak location is confirmed, this lets assume that most of ethane ice stays

at very low temperature and rarely reaches 60K, due to the irreversibility of the crystalline phase. The position of the three more reliable ethane ice bands agrees with pure ethane ice rather than diluted ethane ice in nitrogen (see Table 5). This suggests that ethane ice is preferentially located in the methane ice rich areas. This agrees with the work of Moore & Hudson (2003) who report much larger amount of ethane ice after irradiation of pure methane ice compared to that obtained with methane ice diluted in nitrogen.

Table 5 must appear here

The depth of the ethane ice bands reach 0.015 in albedo (see Table 5). This confirms that small amounts of ethane ice are present on the superficial layers of Pluto. The absorption bands in the H band are less obvious (see Figure 14, lower part), maybe because they are weaker and narrower, but the absorption features of ethane at 1.689, 1.698, 1.738 and 1.764μ seem quite reliable. We do not report the absorption band of diluted ethane ice at 1.755μm (Quirico & Schmitt 1997), in agreement with our previous analysis on the ethane ice form performed in the spectroscopic K band. This could suggest that ethane is predominantly associated with methane ice particles, which are the parent species (Baratta et al. 2002; Moore et al. 2007). Moreover, we detect more easily the ethane absorption bands in those of methane ice in the K band, which are close to saturation. This could suggest stratification of ethane, predominantly present on the topmost layer of methane.

4.5. Search for other compounds

The absorption bands at 2.35μm seems mainly due to CO. Unfortunately, we are not able to distinguish ^{13}CO, due to the position of ^{13}CO (at 2.4050μm and blended with ethane absorption bands). Table 5 reports the properties of the strongest band of CO in our wavelength range. Figure 16 shows the absorption feature of the 2.352μm after continuum

removal. The spectral model used to remove the continuum is presented in Figure 15 (with only methane ice as volatile compound). The absorption depth is close to 0.04±0.01 in albedo and the position of the band is that of pure CO from Quirico & Schmitt (1997). The authors report that wavelength shifts of the absorption bands of diluted CO are very small compared to those of pure CO ice and our spectral resolution does not allow us to constrain the form of CO.

Figure 16 must appear here

We detect an absorption band near 1.58μm, which seems slightly shifted to a longer wavelength, within the errors, compared to the CO absorption band (see Table 5). This feature is reported only during the second night, with the less noisy data. New observations are needed to confirm this absorption band because the measured band depth is the half of the 2.352μm one, although the absorption coefficient of the CO band at 1.59μm is more than 200 times lower. This band could be due to other compound, such as CO_2. However, the absorption band position of CO_2 is different (see Figure 17, panel a). The absorption bands in the 1.9-2.1μm range are not identified, after continuum removal. To remove the continuum, we use a linear regression between the boundaries of each wavelength range reported in Figure 17. We expect the main stellar and telluric lines well removed within 1 to 2% (see in Figure 9). The amount of CO_2 should be negligible.

Figure 17 must appear here

5. Discussion

The observations of Charon seem to confirm the presence of hydrated ammonia in different amounts (due to different absorption band depth) and different physical states (at

different locations) on the surface of Charon. According to our results and those of Cook et al. (2007), it is possible that the anti-Pluto surface is covered with more hemihydrates than the sub-Pluto surface and that ammonia species are more abundant in the leading side (Dumas et al. 2001). From laboratory measurements, performed by Grundy & Schmitt (1998), or Mastrapa et al. (2008) for instance, the strong 1.65μm absorption band indicates that the water ice is almost completely in its crystalline form on the surface of Charon. Therefore, this band allows us to perform a remote temperature sensing (Grundy & Schmitt 1998; Merlin et al. 2007). The position of the crystalline water ice is 1.6548$\pm$0.0006μm for both nights, with absorption band depth of 24.42$\pm$1.63% (FWHM: 0.0230$\pm$0.0015μm) and 25.21$\pm$1.72% (FWHM: 0.0252$\pm$0.0017μm) for the first and second night, respectively. This suggests a mean surface temperature close to 50$\pm$12K for the anti-Pluto surface, consistent with the value derived by Cook et al. (2007) (1.6545$\pm$0.0008μm, i.e., 54K). Our results suggest some chemical surface variations on the anti-Pluto surface because Cook et al. (2007) found a different FWHM (0.031$\pm$0.003μm). Because the polar angle has changed between the two observations, we cannot make any conclusions on the temporal or/and geographical variations. The ammonium component seems to fluctuate on the surface and a complete rotational study is required. All these results are puzzling and it is obvious that the models are still limited in order to derive the detailed chemical composition of Charon's surface. Laboratory measurements of diluted ammonia in different stoichiometric forms are required to fully sample the best candidates which should allow us to match the strong feature at 1.65μm, and the smallest ones near 2.0 and 2.21μm. A complete rotational survey is also required to identify the 2.24μm band, tentatively assigned to the ammonium ion NH_4^+. This feature is not reported in our observations but comparisons between leading and trailing sides are very encouraged to constrain its formation.

The question of a recent or continuous volatile transport on the surface of Pluto is still under debate. Indeed, Grundy & Buie (2001) and Buie et al. (1997), from long-term

photometric measurements, do not find any evidence of this kind of phenomena. On the contrary, the authors suggest that the light curve results from a purely geometrical effect. However, detection of abundant methane quantities in the atmosphere of Pluto has been recently confirmed in the thin N_2 rich atmosphere of the dwarf planet (see Lellouch et al. 2009). This implies warmer temperatures in the atmosphere, close to 60K, and highly probable vents and volatile transport on the surface. Moreover, Doute et al. (1999) offer a scenario to explain their spectroscopic results, with a stratification of the methane ice and nitrogen ice layers. They suggest a seasonal transport of the volatile species from the warmer to the cooler areas. The more volatile species, as CO or N_2, should condensate in the coldest areas while the CH_4 condensation areas should be closer to the sub-solar point. At the same time, during the sublimation processes, a part of the methane diluted in the nitrogen matrix, leads to form a methane crust of several tens to hundreds of micrometers. The abundance of CH_4 found in the atmosphere (1%, recently confirmed by Lellouch et al. 2009) also implies that pure CH_4 patches must have covered a part of the surface, formed by several seasonal condensations. In order to search for information on the transport of volatiles in the case of Pluto, we need to compare the spectra obtained from the same side of Pluto at different times. Doute et al. (1999) obtained the spectrum of Pluto for a longitude close to 66° in 1995 (i.e. very close to the observations obtained the first night). As the pole inclination has changed (-15 to -41°), there is an 86% overlap of the surface observed by Doute et al. (1999) and our observations, that is larger than the identical area covered by both of our observations (74% of the area), that give very similar patterns. We have no large differences of peak positions between the two nights and both spectra are in agreements with a mean CH_4:N_2 ratio greater than 2% (see Figure 8). At the same longitude in 1995, the peak positions of the methane ice bands in the H spectroscopic band match those of the diluted state, from Doute et al. (1999), that suggest probable variation of the dilution state of methane ice. Our cumulative results on the peak position bands

and the presence of pure methane ice support the presence of pure methane ice patches on Pluto. From these results, we agree with the model of Doute et al. (1999) suggesting that pure methane ice (with grain sizes of several hundreds of μm) could be present on top of a diluted rich N_2 matrix close to the warmest areas. Layers of re-deposited pure or mixed nitrogen should be close to the coldest areas and several patches of pure or diluted materials could be present in both areas (with some patches of thick methane ice layers). A spatial investigation should provide some valuable constraints on that subject.

The investigation of the irradiated products on Pluto's surface, suggests that overall, we find mostly heavily irradiated products (such as Titan Tholin) rather than direct irradiated products (such as ethane or ethylene). Indeed, our spectral models agree with around 20% of Titan Tholin and less than 5% of ethane. It is probable that most of the irradiated products are formed in the nitrogen rich atmosphere of Pluto, similarly to the processes expected in the atmosphere of Titan. The surface of Pluto could be shielded from space weathering by this thin atmosphere during the perihelion. At larger heliocentric distances, when the atmosphere is thinner or inexistent, the large amount of re-deposited nitrogen on the surface may partly inhibit the production of ethane or ethylene. This hypothesis is well supported by the observation of ethane mainly in its pure state and probably mixed with the topmost layers of methane. In this scenario, most of the patches of pure methane ice, suggested and confirmed in this work, could be covered by nitrogen ice at longest distance, when the temperature drops. The stratification of ethane could possibly occur during the sublimation and re-condensation processes along the eccentric orbit of Pluto. Ethane could be mainly formed close to the aphelion (thinner atmosphere) on the top of the methane ice rich patches, not or partially covered by nitrogen. When Pluto reaches its perihelion, nitrogen and methane can sublimate and be re-deposited on the surface, gradually covering the layers including ethane. In this scenario, most of ethane should be masked and the detected ethane should be formed recently (a few Plutonian years). Ethane could also be

deposited to the surface by precipitation from the atmosphere of Pluto (Krasnopolsky & Cruikshank 1999). In this model, on the contrary, the maximum production rate is expected close to the perihelion. In-situ observations, lead by the NEW HORIZONS spacecraft in 2015, should give us constrains on these scenarios. Presence of other CH_4 and N_2 daughter species as C_2H_2, C_4H_2, HC_3N and HCN are expected from irradiation (i.e. Gerakines et al. 1996; Krasnopolsky & Cruikshank 1999; Moore & Hudson 2003). CH_2CHCN has been mentioned by Protopapa et al. (2008) based on observations performed between 4.5 and 5.0mum. Higher signal-to-noise data are required to search for these compounds.

6. Conclusions

From our photometric and spectroscopic observations, we were able to define the first near IR photometry of each object for east longitude close to 5°/-41° for Pluto and 185°/-41° for Charon. By spectroscopy, we confirm the heterogeneous nature of the surface of both objects, particularly on the amount and the properties of the hydrated ammonia for Charon and the diluted level of the methane ice for Pluto. Amorphous water ice seems to be depleted and most of the water ice is probably in its crystalline form on Charon. For Pluto, the models suggest a large quantity of irradiated material such as Titan Tholin. Most of these products can be formed in the thin nitrogen-dominated atmosphere. Small amounts of ethane are detected in the two H and K spectroscopic bands, and our work suggests a possible ethane life cycle on the surface of Pluto. CO_2 ice is not detected on the spectra of this object. The temporal variations on the methane ice properties on Pluto are also likely supported from our analyses. This confirms the hypothesis of Doute et al. (1999) and the observations of Lellouch et al. (2009) on the volatile transportation (N_2, CH_4 and CO) and on the presence of pure methane ice patches on the surface of this object. New observations with a better spatial resolution are needed to investigate on the heterogeneous

and temporal evolution of the surface of the two objects.

Acknowledgments: We are very grateful to the two anonymous referees for their valuable comments that contributed to the improvement of this paper.

REFERENCES

Baratta, G. A., Leto, G., & Palumbo, M. E., 2002, A comparison of ion irradiation and UV photolysis of CH_4 and CH_3OH. A&A, 384, 343-349

Barkume, K. M., Brown, M. E., & Schaller, E. L., 2008, Near-Infrared Spectra of Centaurs and Kuiper Belt Objects, AJ, 135, 55-67

Barucci, M. A., Boehnhardt, H., Dotto, E., Doressoundiram, A. , Romon, J., Lazzarin, M., Fornasier, S., de Bergh, C., Tozzi, G. P., Delsanti, A., Hainaut, O., Barrera, L., Birkle, K., Meech, K., Ortiz, J. L., Sekiguchi, T., Thomas, N., Watanabe, J., West, R. M., & Davies, J. K., 2002, Visible and near-infrared spectroscopy of the Centaur 32532 (2001 PT_{13}). ESO Large Program on TNOs and Centaurs: First spectroscopy results. A&A, 392, 335-339

Barucci, M. A., Merlin, F., Guilbert, A., de Bergh, C., Alvarez-Candal, A., Hainaut, O., Doressoundiram, A., Dumas, C., Owen, T, & Coradini, A., 2008, Surface composition and temperature of the TNO Orcus, A&A, 479, L13-L16

Brown, R. H., Cruikshank, D. P., Tokunaga, A. T., Smith, R. G., & Clark, R. N., 1988, Search for volatiles on icy satellites. I - Europa . Icarus, 74, 262-271

Brown, M. E., & Calvin, W. M., 2000, Evidence for Crystalline Water and Ammonia Ices on Pluto's Satellite Charon. Science, 287, 107-109

Brown, M. E., Schaller, E. L., Roe, H. G., Rabinowitz, D. L., & Trujillo, C. A., 2006, Direct Measurement of the Size of 2003 UB313 from the Hubble Space Telescope . ApJ, 643, L61-L63

Brunetto, R., Barucci, M. A., Dotto, E., & Strazzulla, G., 2006, Ion Irradiation of

Frozen Methanol, Methane, and Benzene: Linking to the Colors of Centaurs and Trans-Neptunian Objects, ApJ, 644, 646-650

Buie, M. W., Tholen, D. J., & Wasserman, L. H., 1997, Separate Lightcurves of Pluto and Charon . Icarus, 125, 233-244

Buratti, B. J. , Hillier, J. K., Heinze, A., Hicks, M. D., Tryka, K. A., Mosher, J. A., Ward, J., Garske, M., Young, J., & Atienza-Rosel, J., 2003, Photometry of Pluto in the last decade and before: evidence for volatile transport? Icarus, 162, 171-182

Cook, J. C., Desch, S. J., Roush, T. L., Trujillo, C. A., & Geballe, T. R., 2007, Near infrared spectroscopy of Charon. Possible evidence for cryovolcanism on Kuiper Belt Objects. ApJ, 663, 1406-1419

Cook, J. C., Olkin, C. B., Desch, S. J., Mastrapa, R. M., Roush, T. L., & Verbiscer, A. J. ; 2009, Examination of the K-Band Spectrum of Charon: Possible Evidence for Multiple Ammonia Ices. LPI Science Conference Abstracts, 40, 2222

Cruikshank, D. P., Pilcher, C. B., & Morrison, D., 1976, Pluto - Evidence for methane frost . Science, 194, 835-837

Cruikshank, D. P., Owen, T. C., Ore, C. D., Geballe, T. R., Roush, T. L., de Bergh, C., Sandford, S. A., Poulet, F., Benedix, G. K., & Emery, J. P., 2005, A spectroscopic study of the surfaces of Saturn's large satellites: H_2O ice, tholins, and minor constituents . Icarus, 175, 268-283

Dalle Ore, C. M., Barucci, M. A., Emery, J. P., Cruikshank, D. P., Dalle Ore, L. V., Merlin, F., Alvarez-Candal, A., de Bergh, C., Trilling, D. E., Perna, D., Fornasier, S., Mastrapa, R. M. E., & Dotto, E., 2009, Composition of KBO (50000) Quaoar. A&A, 501, 349-357

de Bergh, C., Boehnhardt, H., Barucci, M.A., Lazzarin, M., Fornasier, S., Romon-Martin, J., Tozzi, G.P., Doressoundiram, A. & Dotto, E., 2004, Aqueous altered silicates at the surface of two Plutinos? A&A, 416, 791-798

DeMeo, F.E., Dumas, C., de Bergh C., Protopapa, S., Cruikshank ; D.P., Geballe, T.R., Alvarez-Candal, A., Merlin, F., Barucci M.A., 2010, A search for ethane on Pluto and Triton, Icarus 208, 412-424.

Douté, S., Schmitt, B., Quirico, E., Owen, T. C., Cruikshank, D. P., de Bergh, C., Geball, T. R., & Roush, T. L. 1999, Evidence for Methane Segregation at the Surface of Pluto. Icarus, 142, 421-444

Dumas, C., Terrile, R. J., Brown, R. H., Schneider, G., & Smith, B. A., 2001, Hubble Space Telescope NICMOS Spectroscopy of Charon's Leading and Trailing Hemispheres. AJ, 121, 1163-1170

Dumas, C., Merlin, F., Barucci, M. A., de Bergh, C., Hainault, O., Guilbert, A., Vernazza, P., & Doressoundiram, A., 2007, Surface composition of the largest dwarf planet 136199 Eris (2003 UB_{313}). A&A, 471, 331-336

Dumas, C., Carry, B., Merlin, F., Hestroffer, D., Vernazza, P., & Kaasalainen, M. 2009, Spatially Resolved Observations of Small Solar System Bodies. BAAS, 41, #68.15

Gerakines, P. A., Schutte, W. A., & Ehrenfreund, P. 1996, Ultraviolet processing of interstellar ice analogs. I. Pure ices. A&A, 312, 289-305

Goldberg, L., Mohler, O. & McMath, R., 1948, The Solar Corona and Ultraviolet Radiation . Harvard Observatory Monographs vol. 7

Grundy, W. M., & Schmitt, B., 1998, The temperature-dependent near-infrared absorption spectrum of hexagonal H_2O ice, J. Geophys. Res., 103, 25809-25822

Grundy, W. M., & Buie, M. W. 2001, Distribution and Evolution of CH_4, N_2, and CO Ices on Pluto's Surface: 1995 to 1998 . Icarus, 153, 248-263

Grundy, W. M., Schmitt, B., & Quirico, E. 2002, The Temperature-Dependent Spectrum of Methane Ice I between 0.7 and 5μm and Opportunities for Near-Infrared Remote Thermometry . Icarus, 155, 486-496

Hapke, B., 1981, Bidirectional reflectance spectroscopy. 1. Theory, J. Geophys. Res., 86, 4571-4586

Hapke, B., 1993,Theory of reflectance and emittance spectroscopy, Topics in Remote Sensing, Cambridge, UK: Cambridge University Press, —c1993,

Hudson, R. L., Moore, M. H., & Raines, L. L. 2009, Ethane ices in the outer Solar System: Spectroscopy and chemistry . Icarus, 203, 677-680

Jewitt, D. C., & Luu, J.X., 2001, Colors and Spectra of Kuiper Belt Objects, AJ, 122, 2099-2114

Jewitt, D. C., & Luu, J., 2004, Crystalline water ice on the Kuiper belt object (50000) Quaoar. Nature, 432, 731-733

Khare, B. N., Sagan, C., Ogino, H., Nagy, B., Er, C., Schram, K. H., & Arakawa, E. T., 1986, Amino acids derived from Titan tholins, Icarus, 67, 176-184

Krasnopolsky, V. A., & Cruikshank, D. P. 1999, Photochemistry of Pluto's atmosphere and ionosphere near perihelion. J. Geophys. Res., 104, 21979-21996

Lellouch, E., Sicardy, B., de Bergh, C., Käufl, H.-U., Kassi, S., & Campargue, A. 2009, Pluto's lower atmosphere structure and methane abundance from high-resolution spectroscopy and stellar occultations. A&A, 495, L17-L21

Licandro, J., Pinilla-Alonso, N., Pedani, M.,Oliva, E., Tozzi, G. P., & Grundy, W. M., 2006, The methane ice rich surface of large TNO 2005 FY_9: a Pluto-twin in the trans-neptunian belt? A&A, 445, L35-L38

Mastrapa, R. M., Bernstein, M. P., Sandford, S. A., Roush, T. L., Cruikshank, D. P., & Ore, C. M. D., 2008, Optical constants of amorphous and crystalline H_2O-ice in the near infrared from 1.1 to 2.6 μm, Icarus, 197, 307-320

Merlin, F., Guilbert, A., Dumas, C., Barucci, M. A., de Bergh, C., & Vernazza, P., 2007, Properties of the icy surface of the TNO 136108 (2003 EL_{61}), A&A, 466, 1185-1188

Merlin, F., Alvarez-Candal, A., Delsanti, A., Fornasier, S., Barucci, M. A., DeMeo, F. E., de Bergh, C., Doressoundiram, A., Quirico, E., & Schmitt, B., 2009, Stratification of Methane Ice on Eris' Surface, AJ, 137, 315-328

Moore, M. H., & Hudson, R. L. 2003, Infrared study of ion-irradiated N_2-dominated ices relevant to Triton and Pluto: formation of HCN and HNC. Icarus, 161, 486-500

Moore, M. H., Ferrante, R. F., Hudson, R. L., & Stone, J. N. 2007, Ammonia water ice laboratory studies relevant to outer Solar System surfaces. Icarus, 190, 260-273

Olkin, C. B., Young, E. F., Young, L. A., Grundy, W., Schmitt, B., Tokunaga, A., Owen, T., Roush, T., Terada, H., 2007, Pluto's Spectrum from 1.0 to 4.2 μm: Implications for Surface Properties. AJ, 133, 420-431

Owen, T. C., Roush, T. L., Cruikshank, D. P., Elliot, J. L., Young, L. A. de Bergh, C., Schmitt, B., Geballe, T. R., Brown, R. H., & Bartholomew, M. J., 1993, Surface ices and the atmospheric composition of Pluto. Science, 261, 745-748

Pickles, A. J. 1998, A Stellar Spectral Flux Library: 1150-25000 Å. PASP, 110, 863-878

Poulet, F., Cuzzi, J. N., Cruikshank, D. P., Roush, T., & Dalle Ore, C. M., 2002, Comparison between the Shkuratov and Hapke Scattering Theories for Solid Planetary Surfaces: Application to the Surface Composition of Two Centaurs, Icarus, 160, 313-324

Protopapa, S., Boehnhardt, H., Herbst, T. M., Cruikshank, D. P., Grundy, W. M., Merlin, F., & Olkin, C. B., 2008, Surface characterization of Pluto and Charon by L and M band spectra. A&A, 490, 365-375

Quirico, E., & Schmitt, B., 1997, Near-Infrared Spectroscopy of Simple Hydrocarbons and Carbon Oxides Diluted in Solid N_2 and as Pure Ices: Implications for Triton and Pluto. Icarus, 127, 354-378

Quirico, E., Doute, S., Schmitt, B., de Bergh, C., Cruikshank, D. P., Owen, T. C., Geballe, T. R., & Roush, T. L., 1999, Composition, Physical State, and Distribution of Ices at the Surface of Triton. Icarus, 139, 159-178

Romon, J., de Bergh, C., Barucci, M. A., Doressoundiram, A., Cuby, J.-G., Le Bras, A., Douté, S., & Schmitt, B., 2001, Photometric and spectroscopic observations of Sycorax, satellite of Uranus. A&A, 376, 310-315

Schaller E.L., & Brown, M.E., 2007, Volatile Loss and Retention on Kuiper Belt Objects ApJ, 659, L61-L64

Strazzulla, G., Cooper, J.F., Christian, E.R., & Jonhson, R.E., 2003, Ion irradiation of TNOs: from the fluxes measured in space to the laboratory esperiments. Comptes rendus de l'academie des sciences Vol 4, 791-802

Tegler, S. C., Bauer, J. M., Romanishin, W., & Peixinho, N., 2008, Colors of Centaurs. The Solar System Beyond Neptune, University of Arizona Press, Tucson, 105-114

Verbiscer, A., & Helfenstein, P., 1998, Reflectance Spectroscopy of Icy Surfaces, Solar System Ices, 227, 157-198

Zubko, V. G., Mennella, V., Colangeli, L., & Bussoletti, E., 1996, Optical Constants of Amorphous Carbon Extracted from Recent Laboratory Extinction Measurements, The Role of Dust in the Formation of Stars, 333

This manuscript was prepared with the AAS LaTeX macros v5.0.

Table 1: Observational circumstances: Date of the exposures, instruments used, sub-earth longitude and latitude, phase angle (α), heliocentric distance (r) and geocentric distance (Δ).

Date	Inst.[a]	Long/lat[b]	α (°)	r(AU)	Δ(AU)
2008/04/12	F+S	63.0-58.0/-41	1.65	31.44	31.06
2008/04/13	I+S	8.00-3.00/-41	1.65	31.44	31.06

[a]F=FORS2, S=SINFONI, I=ISAAC [b]Sub-Earth longitudes and latitudes during the entire exposition, according to the Olkin et al. (2007) notation.

Table 2: Spectroscopic observations.

Date*	Range (μm)	Exposure Time	Seeing	Airmass	Analog(airmass)
2008 Apr 12, 9:10	0.6-1.0 (F)	2min (6x20s)	0.4”	1.01	HD147935(1.09)
2008 Apr 12, 9:40	1.45-2.45 (S)	20min (8x150s)	0.4”	1.01	SA110361(1.1)
2008 Apr 13, 8:30	1.1-1.35 (I)	6min (12x30s)	0.5”	1.02	HD147935(1.08)
2008 Apr13, 8:40	1.45-2.45 (S)	1hr(12x300s)	0.5”	1.02	HD147935(1.02)

F=FORS2, S=SINFONI, I=ISAAC *Date at start exposure in Universal Time.

Table 3: Photometric Results for 2008 April 13.

Band	J(1.25 μm)	H(1.65 μm)	Ks(2.2 μm)
Pluto	13.14±0.04	13.05±0.04	13.29±0.05
Charon	15.16±0.05	15.14±0.05	15.21±0.06

Table 4: Position peak of pure methane ice bands (in μm) and wavelength shift of the observed absorption bands, and of diluted CH_4 with respect to the pure CH_4 features.

Pure[a]	Apr.12th	Apr.13th	Diluted[a]
0.7296	-0.0013 ± 0.0005		
0.7993	-0.0022 ± 0.0005		
0.8691	-0.0019 ± 0.0005		
0.8897	-0.0020 ± 0.0005		-0.00264
1.1645		-0.0009 ± 0.0004	-0.00315
1.2038		-0.0025 ± 0.0004	
1.3355		-0.0019 ± 0.0004	-0.00334
1.6695	-0.0033 ± 0.0006	-0.0030 ± 0.0005	-0.00392
1.6895	-0.0005 ± 0.0005	-0.0000 ± 0.0005	
1.7245	-0.0022 ± 0.0005	-0.0023 ± 0.0004	-0.00475
1.7966	-0.0021 ± 0.0004	-0.0022 ± 0.0006	-0.00467
2.2081	-0.0039 ± 0.0006	-0.0043 ± 0.0004	-0.00564
2.3234	-0.0050 ± 0.0008	-0.0040 ± 0.0009	-0.00528
2.3793	-0.0046 ± 0.0009	-0.0043 ± 0.0004	-0.00627
2.4295	-0.0038 ± 0.0007	-0.0039 ± 0.0005	-0.00600

[a] from Quirico & Schmitt (1997). Diluted: CH_4:N_2 = 0.02.

Table 5: The properties of the absorption bands corresponding to CO and C_2H_6 detected in the SINFONI Pluto's spectrum are listed. Position and absorption coefficient for the same features as obtained from laboratory measurements (see Quirico & Schmitt 1997) is reported for comparison.

Position (μm)	Depth (albedo)	Compound	Pure[a] Position(μm)	Absorption (cm-1)	Diluted[a] Position(μm)
1.5790±0.0009	2.60±0.90	CO?	1.5780	2.5	
2.2738±0.0030	0.70±0.30	C_2H_6	2.2738	138	2.2690
2.3520±0.0008	4.24±0.96	CO	2.3524	672	
2.4040±0.0020	1.45±0.80	C_2H_6	2.402-2.406[b]	209-228	2.3920
2.4260±0.0030	1.54±0.60	C_2H_6	2.4243	103	2.4140

[a] from Quirico & Schmitt (1997) with CO:N_2=0.01 and C_2H_6:N_2=0.01 [b] Blend of several absorption bands

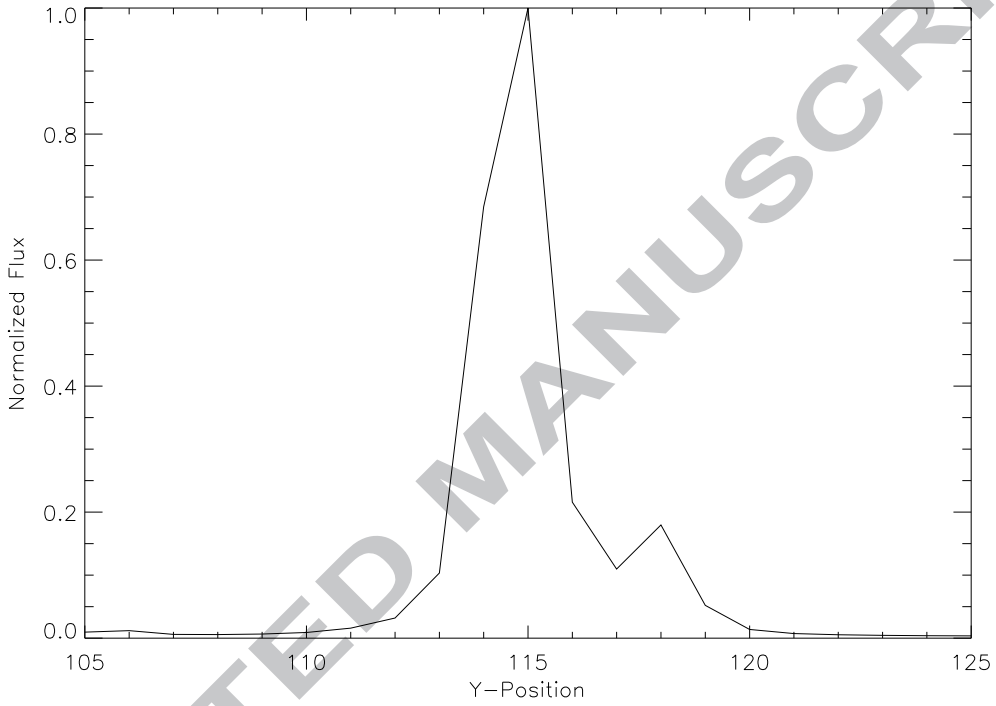

Fig. 1.— Normalized flux profile of the objects along the parralactic angle. Pluto is centered on the 115^{th} pixel while Charon is centered on the 118^{th} pixel.

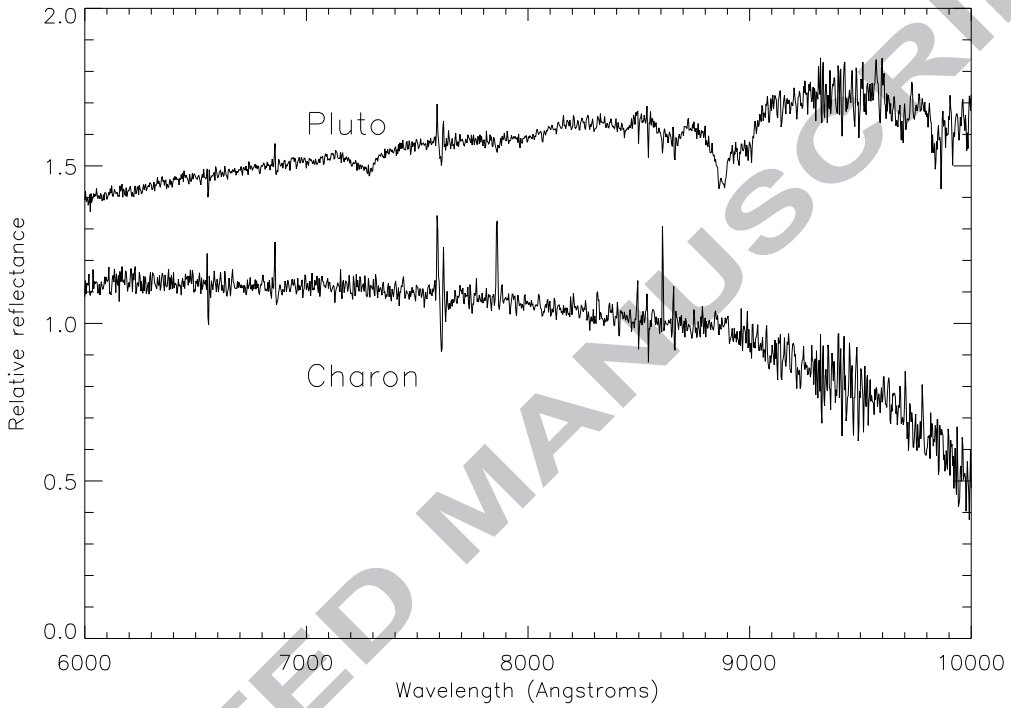

Fig. 2.— Extracted spectra of Pluto and Charon from 0.6 to 1.0 μm (from top to the bottom, respectively). The spectrum of Charon is blue but it is due to a bad background removal (the flux of Pluto is too close).

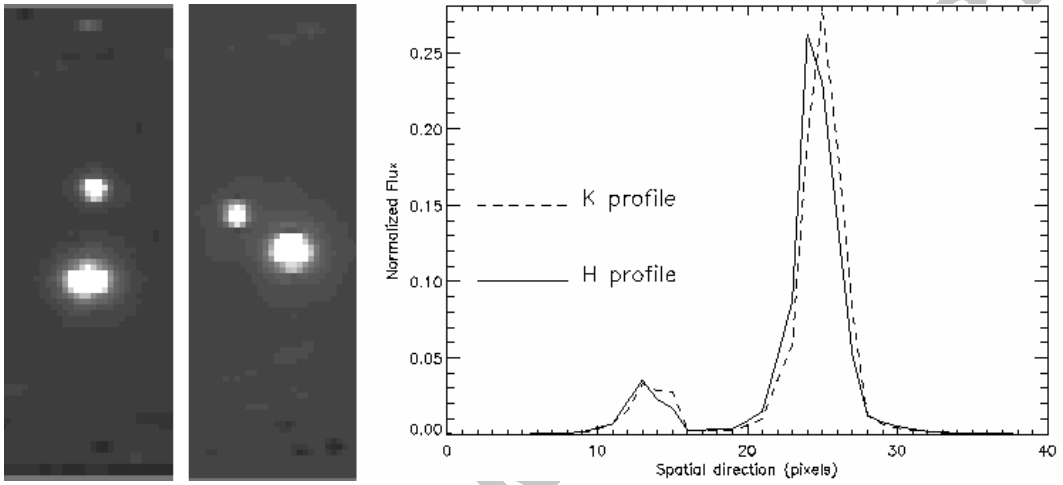

Fig. 3.— Pluto and Charon as seen with SINFONI during the first (on the left image) and second (on the right image) night. Both objects are well separated the first night while a small flux fraction of each object contaminates the other during the second night (less than 3% for Charon and much less than 1% for Pluto), as we can see from the flux profile along the spatial direction in H and K bands corresponding to the second night.

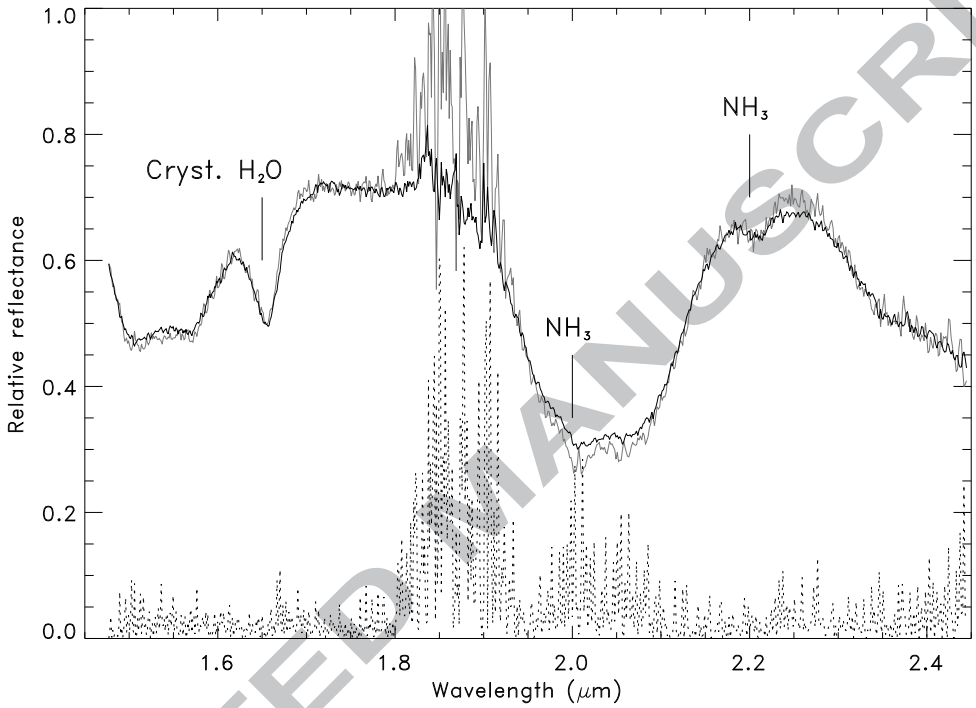

Fig. 4.— Spectra of Charon during both nights (in grey and black for the first and second night, respectively) with the SINFONI instrument. Differences are presented in dotted lines and are small (within 5-10%) except in the telluric absorption band.

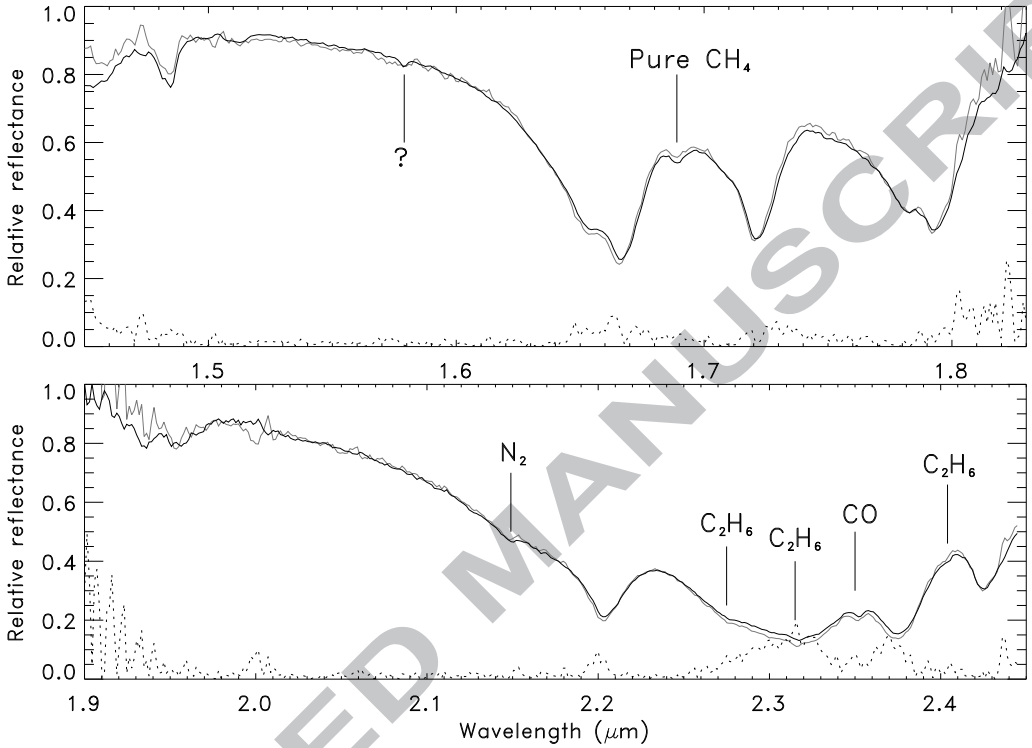

Fig. 5.— Spectra of Pluto during both nights (in grey and black for the first and second night, respectively) with the SINFONI instrument. The difference (in %) is given in dotted line and is mainly within 5%, except in the strongest bands and in the telluric absorption bands.

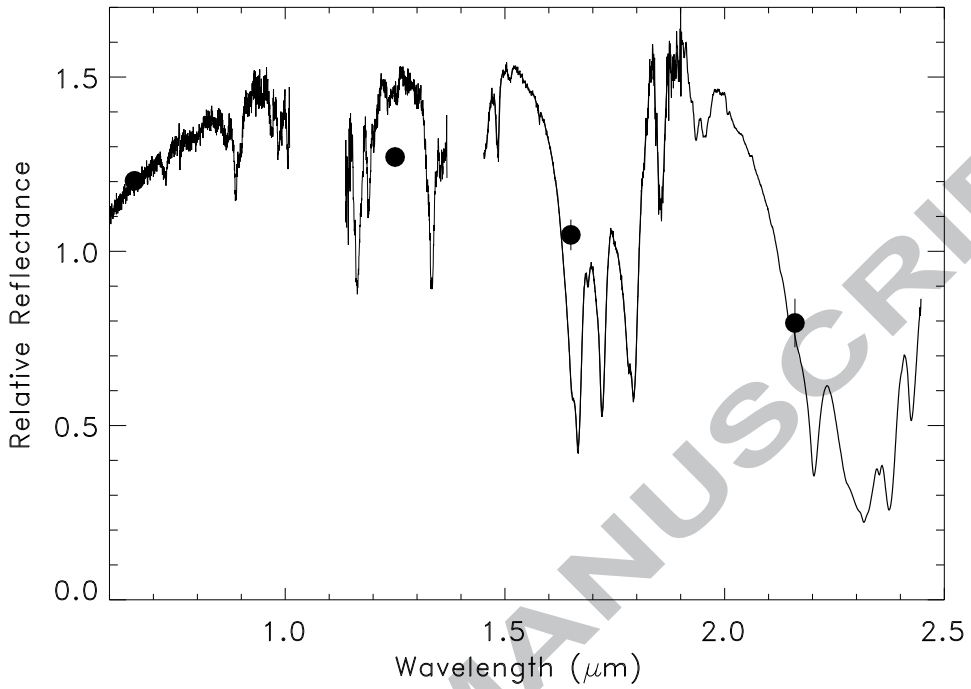

Fig. 6.— Reflectance spectrum of Pluto on the entire 0.6-2.5μm range obtained from the combination of the different spectra normalized at 1 in V band. The visible spectrum has been obtained during the first night and the near-IR spectra during the second night. Black points correspond to the reflectivity obtained in each photometric band (see text for more details).

Fig. 7.— Absorption band near 2.21μm of the Charon spectrum (noisy line) after continuum removal and the fitted Gaussian curve (smooth line).

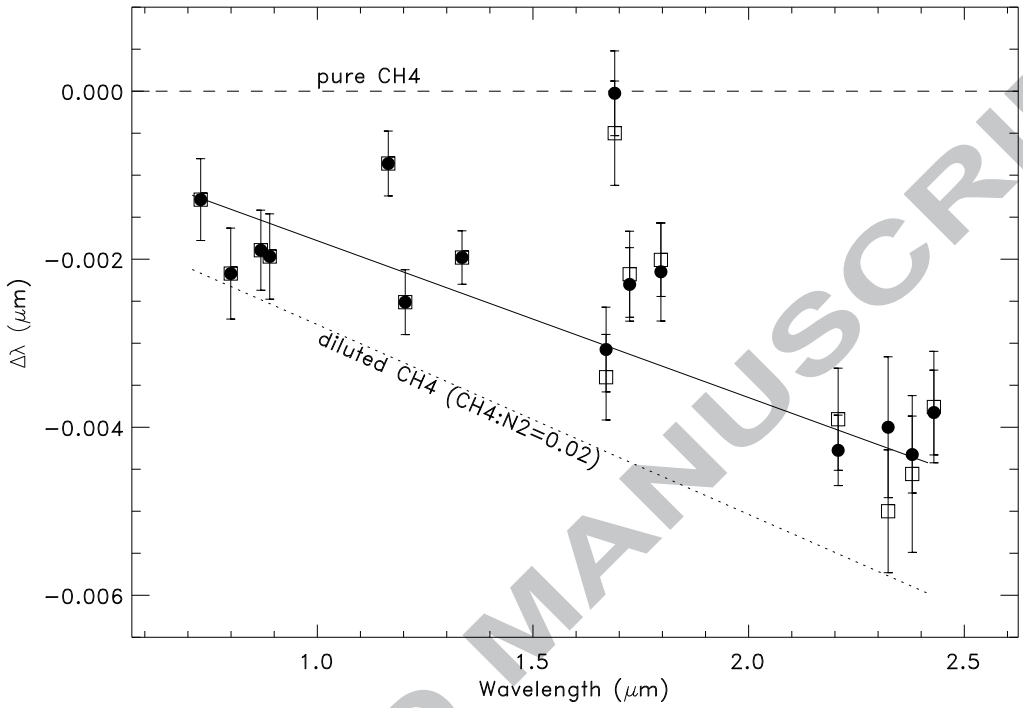

Fig. 8.— Wavelength shifts of the methane ice bands compared to those of pure methane ice for the first and second nights (white squares and black circles, respectively). The position of the 1.689μm of the pure methane ice is not shifted (the dashed line symbolizes the position of pure methane ice bands), within the errors. This shows the good accuracy of the spectral calibration and measurement method. The continuous line is the mean wavelength shift from the different measurements while the dotted line represents the wavelength shift of diluted methane ice (with CH_4:N_2=0.02, from Quirico & Schmitt 1997).

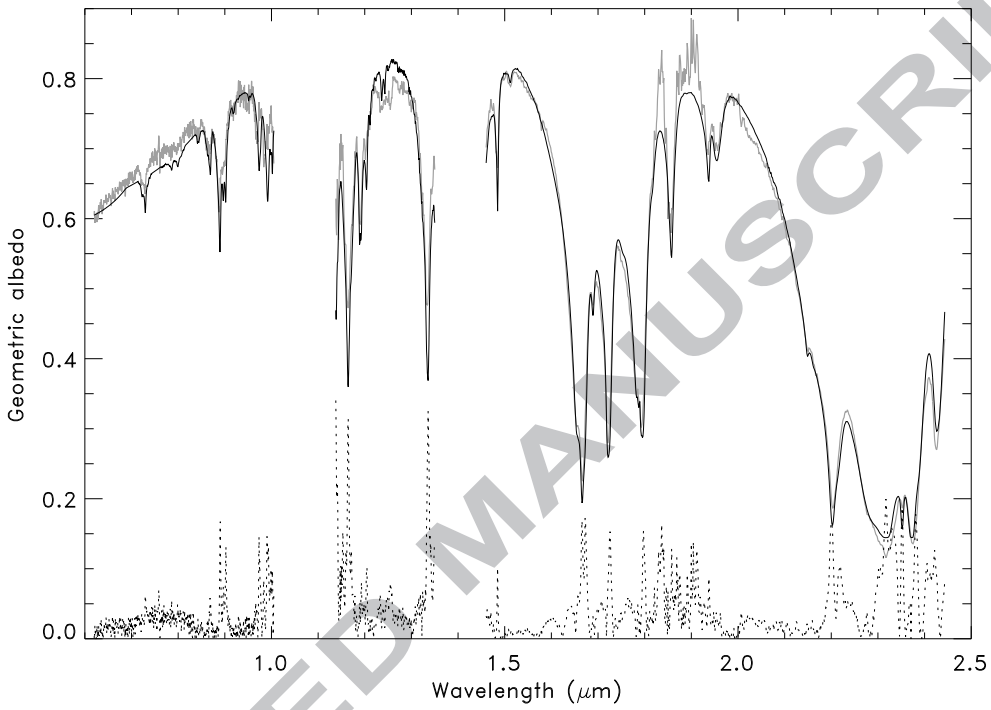

Fig. 9.— Spectrum of Pluto (during the second night with a spectral resolution of 500) and the synthetic model, respectively in grey and black lines. The agreement is within 5%, except in the telluric bands and at the location of the strongest absorption bands (up to 20%). The synthetic spectrum has been obtained assuming **an areal mixture of two areas** (see text).

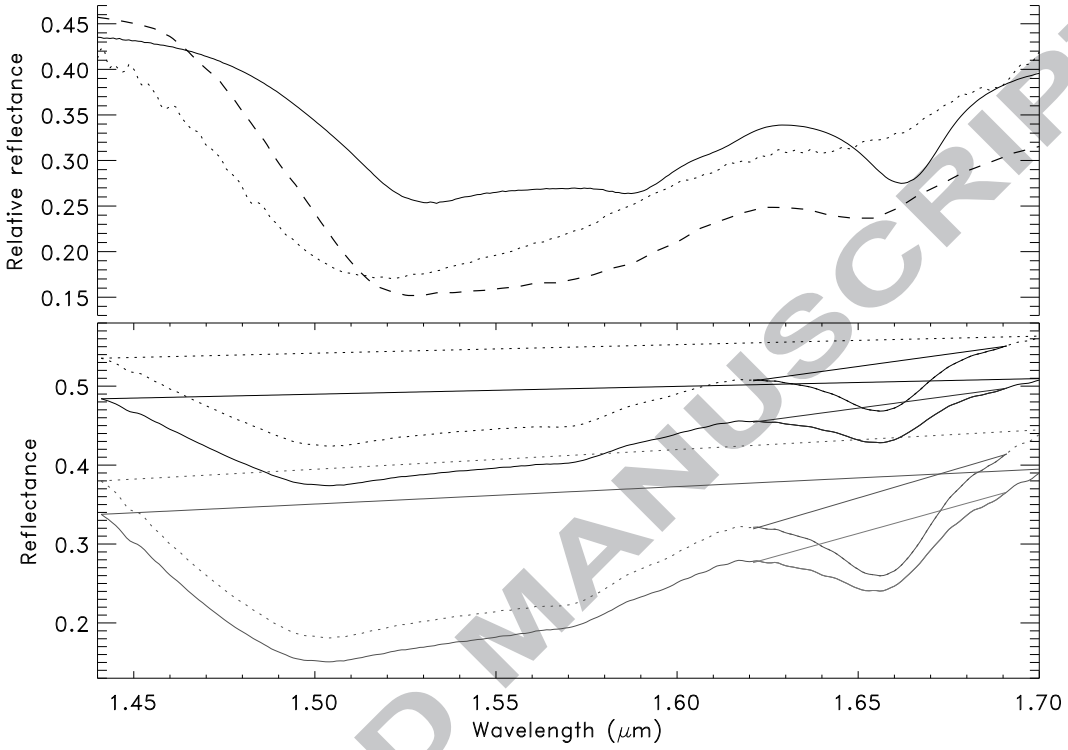

Fig. 10.— Lower panel: Reflectance spectra of a mixture of 50% of amorphous and 50% of crystalline water ice (for particle size of 10 and 100μm, respectively the upper two and lower two curves). The spectra in dotted line are performed using an intimate mixture while the continuous ones are performed using a geographic mixture. The straight lines correspond to the fitted continuum for each band. Upper panel: Synthetic spectra of crystalline (solid line) and amorphous (dotted line) water ice as well as hydrated ammonia (dashed line).

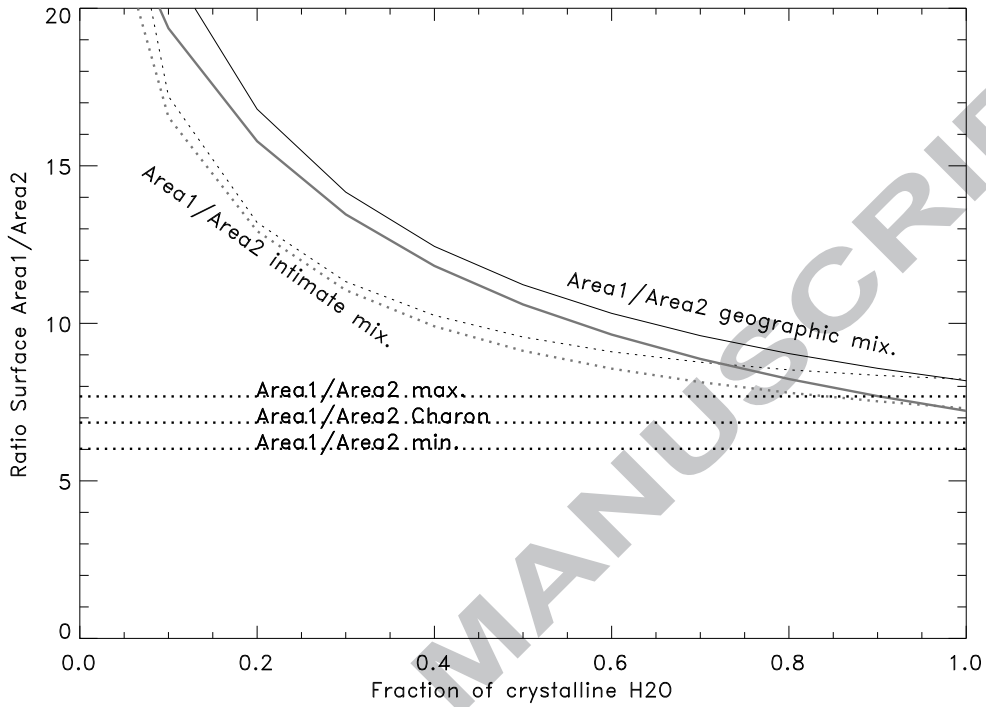

Fig. 11.— Curves of the band area ratio as a function of the fraction of crystalline water ice in the mixture, assuming similar particle sizes of amorphous and crystalline water ice. Dotted lines represent the results for intimate mixture and continuous lines for geographical mixtures. The two different curves for both mixtures are quite similar for two different particle sizes (10 and 100μm, respectively the upper and lower ones) at 50K. The horizontal lines are the median values surrounding by the upper and lower ratio limits computed from the object spectrum. The error on the band surface ratio is obtained considering the spectral noise at 1σ.

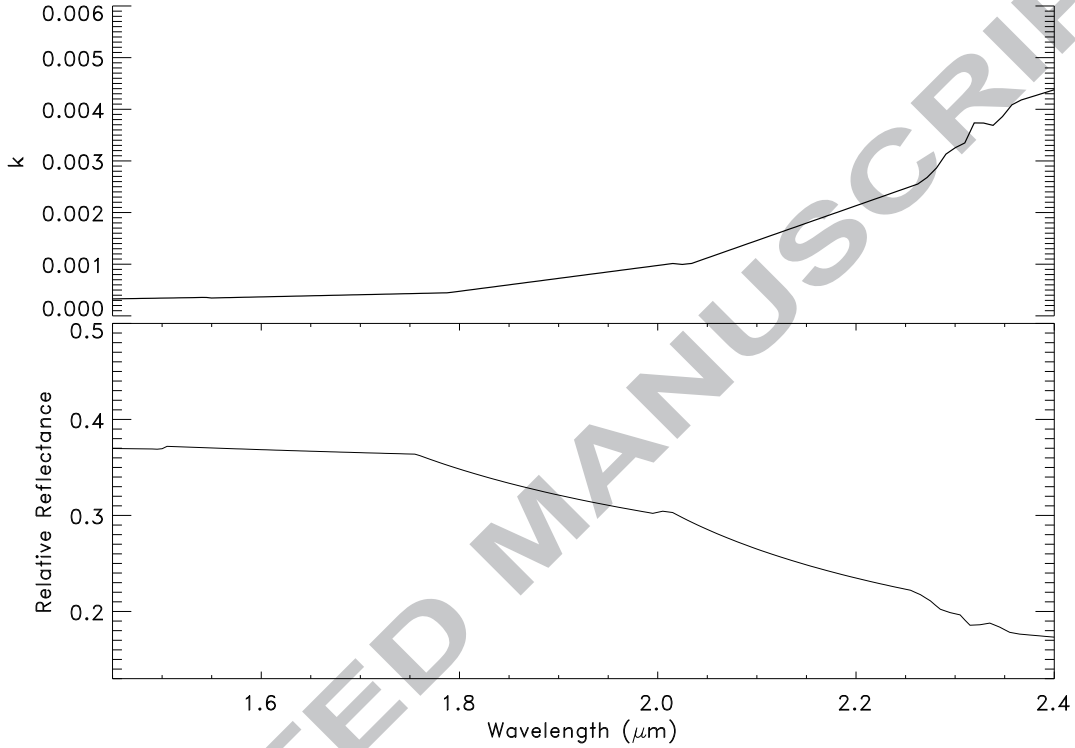

Fig. 12.— Upper panel: Imaginary part of the refraction indices (k) of the component used in our model to reproduce the blue slope of the spectrum of Charon in the near IR. Lower panel: Reflectance of this blue component.

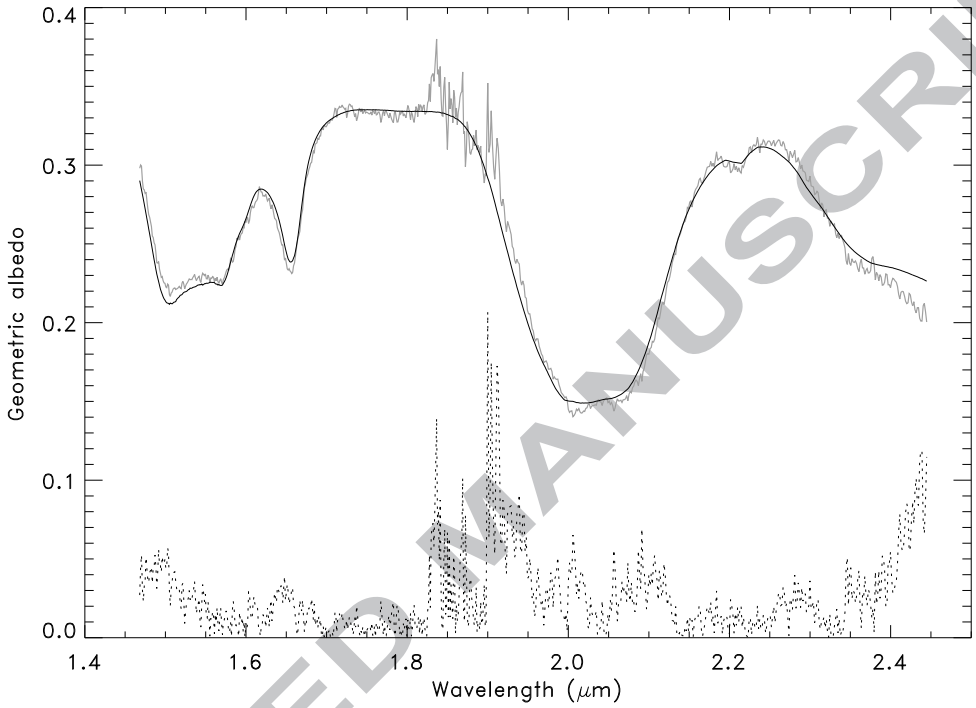

Fig. 13.— Spectra of Charon (during the second night with a spectral resolution of 500) and the synthetic model, respectively in grey and black lines. The differences in % are given by the dotted line. The agreement is within 5%, except in the telluric bands and at the longest wavelengths, where the efficiency of the instrument drops.

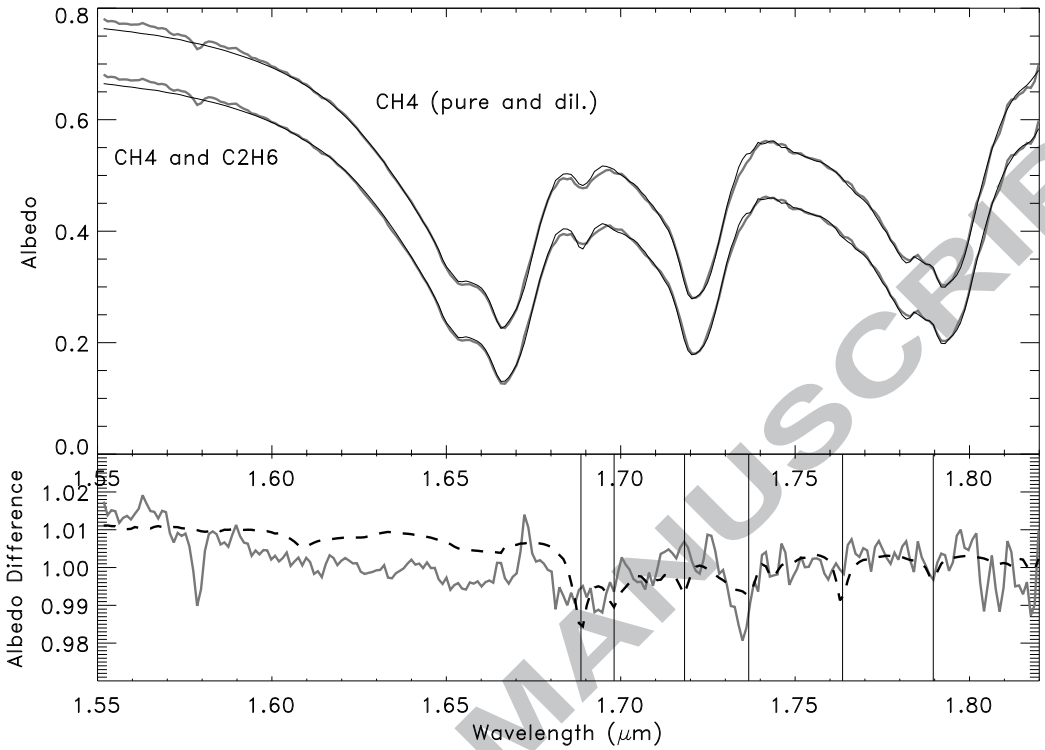

Fig. 14.— In the upper part are presented the spectrum of Pluto and the synthetic models (in gray and black, respectively) including as volatile species, from top to the bottom: 1) pure and diluted methane ice and diluted CO in nitrogen, 2) same as 1) and 3% of ethane. The Object and synthetic spectra are shifted by +0.0 and -0.1 in albedo, respectively, for clarity. In the lower part, the albedo difference between the model without ethane and the object spectrum is presented in gray. A scaled spectrum of Ethane ice, obtained with the Hapke (1981) model and optical constants of Quirico & Schmitt (1997), is superimposed in dashed line. Position peaks of the strongest ethane bands are presented with vertical gray lines.

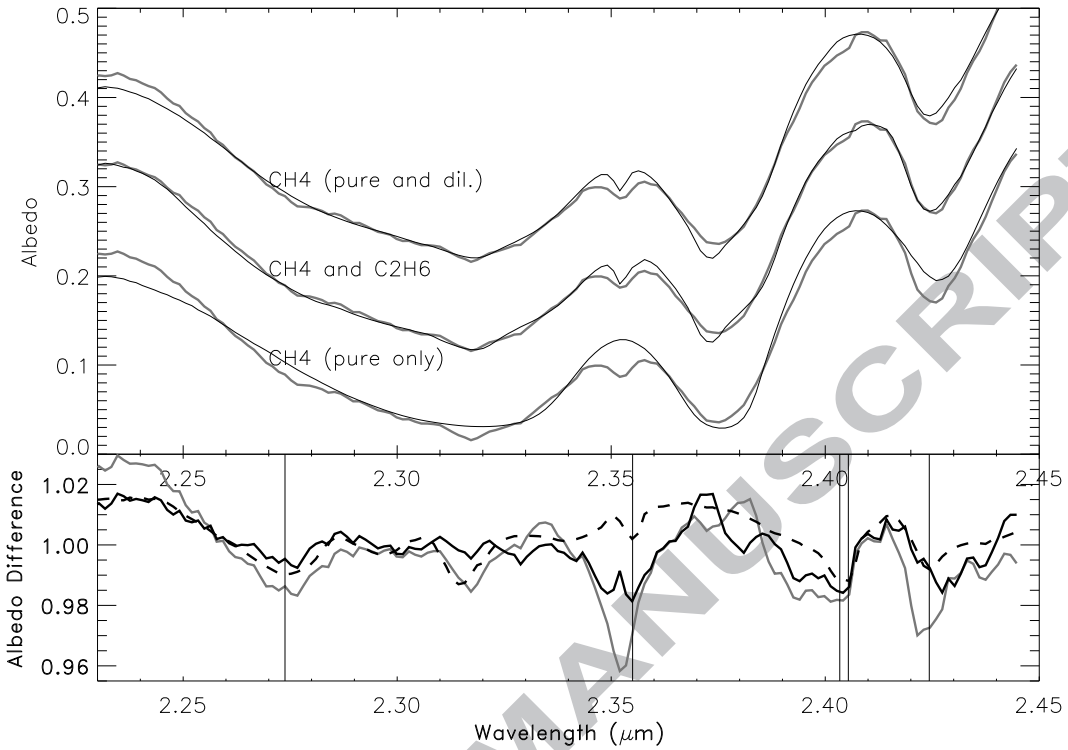

Fig. 15.— In the upper part are presented the spectrum of Pluto and the synthetic models (in gray and black, respectively) including as volatile species, from top to the bottom: 1) pure and diluted methane ice and diluted CO in nitrogen, 2) same as 1) and 5% of ethane 3) pure methane only. The Object and synthetic spectra are shifted by +0.1, +0.0 and -0.1 in albedo, respectively, for clarity. In the lower part, the albedo differences between the models, without ethane, and the object spectrum are presented in black (with diluted CO and methane in nitrogen) and gray (with pure methane ice only). A scaled spectrum of Ethane ice, obtained with the Hapke (1981) model and optical constants of Quirico & Schmitt (1997), is superimposed in dashed line. Position peaks of the strongest ethane bands are presented with vertical gray lines.

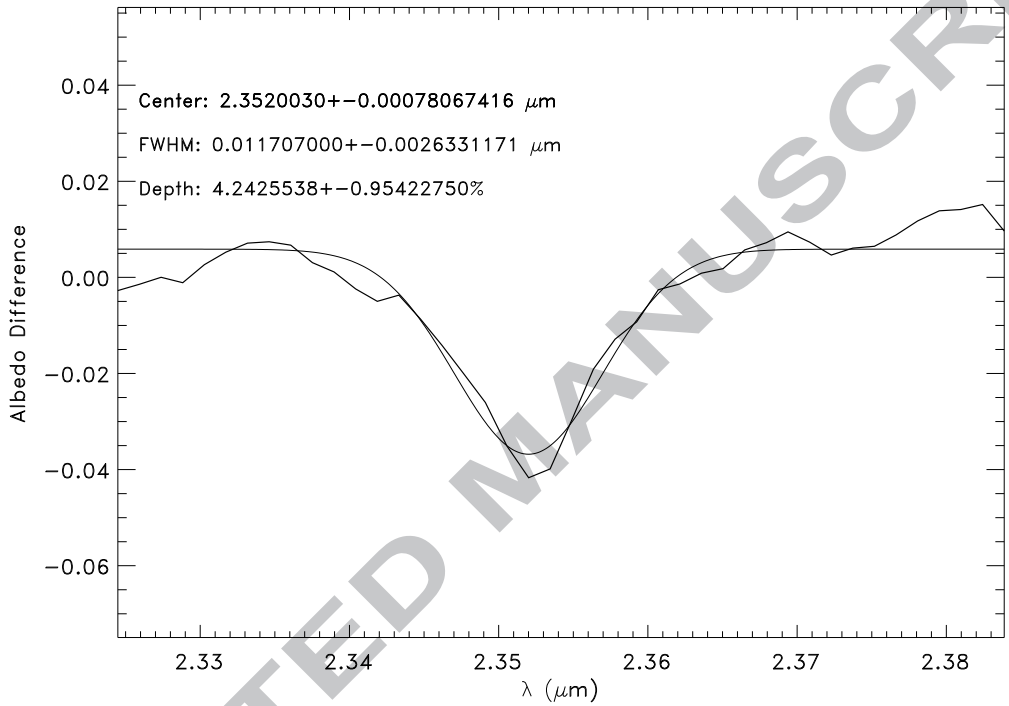

Fig. 16.— Absorption band near 2.35μm of the Pluto spectrum (noisy line) after continuum removal and the fitted gaussian curve (smooth line).

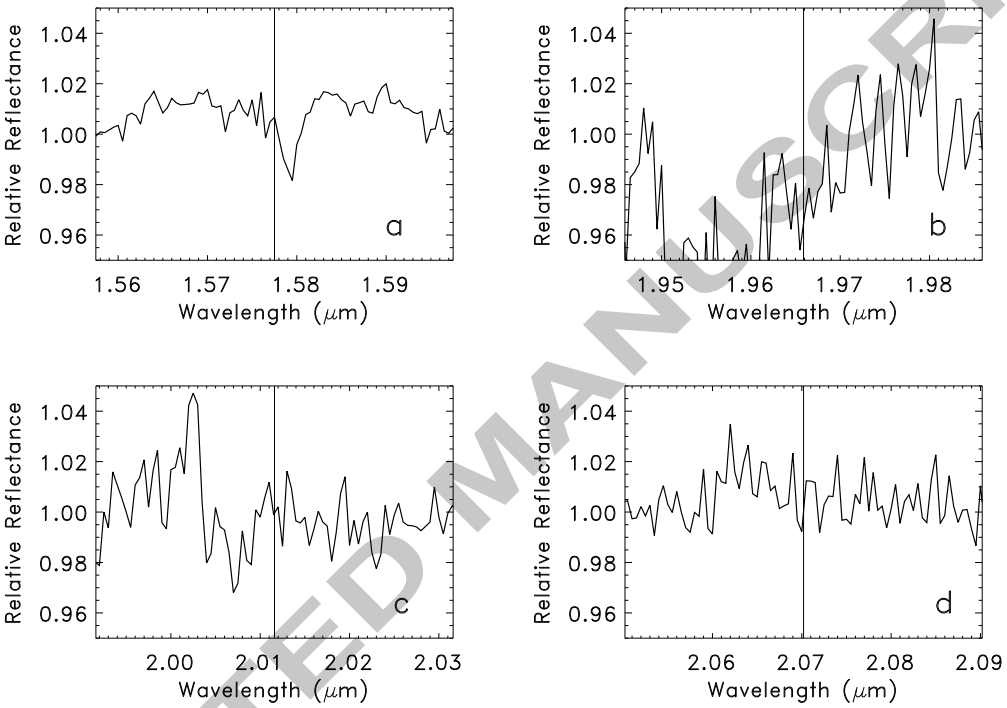

Fig. 17.— Parts of the spectrum of Pluto after continuum removal. The position peak of CO_2 are presented in vertical line.

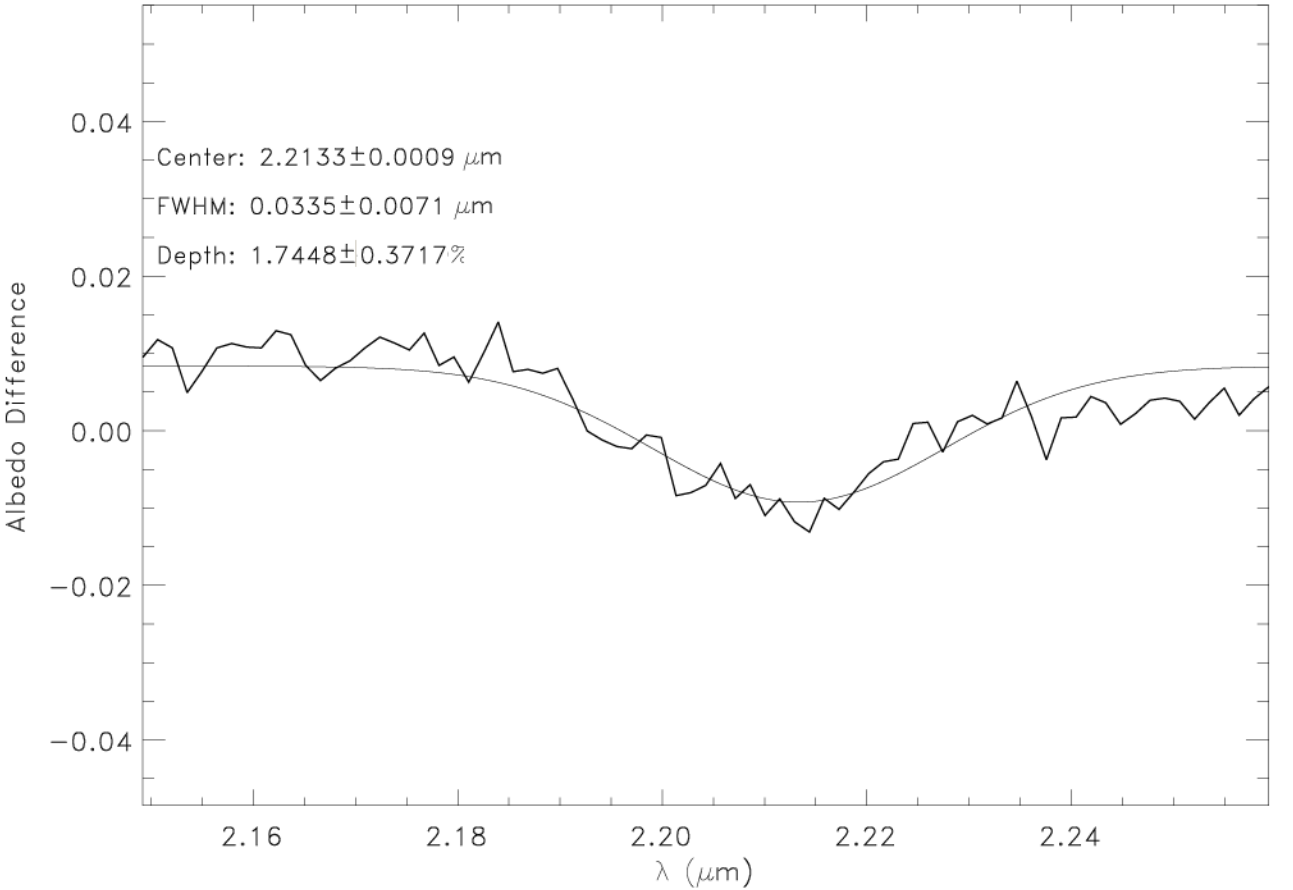
Center: 2.2133±0.0009 μm
FWHM: 0.0335±0.0071 μm
Depth: 1.7448±0.3717%
Albedo Difference
0.04
0.02
0.00
−0.02
−0.04
2.16
2.18
2.20
2.22
2.24
λ (μm)